

This item is likely protected under Title 17 of the U.S. Copyright Law. Unless on a Creative Commons license, for uses protected by Copyright Law, contact the copyright holder or the author.

Access to this work was provided by the University of Maryland, Baltimore County (UMBC) ScholarWorks@UMBC digital repository on the Maryland Shared Open Access (MD-SOAR) platform.

Please provide feedback

Please support the ScholarWorks@UMBC repository by emailing scholarworks-group@umbc.edu and telling us what having access to this work means to you and why it's important to you. Thank you.

RESEARCH ARTICLE

10.1002/2016JA023330

Key Points:

- Integrated energy fluxes vary significantly depending on satellite position with respect to the X line and plasma sheet
- O⁺ enthalpy flux can be a significant or dominant contribution to the overall energy flux from the reconnection region
- Plasma sheet surface waves and drivers of sheet flapping are the primary sources of Poynting flux

Correspondence to:

E. Tyler,
nucko006@umn.edu

Citation:

Tyler, E., C. Cattell, S. Thaller, J. Wygant, C. Gurgiolo, M. Goldstein, and C. Mouikis (2016), Partitioning of integrated energy fluxes in four tail reconnection events observed by Cluster, *J. Geophys. Res. Space Physics*, 121, 11,798–11,825, doi:10.1002/2016JA023330.

Received 13 AUG 2016

Accepted 9 NOV 2016

Accepted article online 16 NOV 2016

Published online 17 DEC 2016

Partitioning of integrated energy fluxes in four tail reconnection events observed by Cluster

Evan Tyler¹, Cynthia Cattell¹, Scott Thaller¹, John Wygant¹, Chris Gurgiolo², Melvyn Goldstein³, and Christopher Mouikis⁴
¹School of Physics and Astronomy, University of Minnesota, Twin Cities, Minneapolis, Minnesota, USA, ²Bitterroot Basic Research, Hamilton, Montana, USA, ³NASA Goddard Space Flight Center, Greenbelt, Maryland, USA, ⁴Space Science Center, University of New Hampshire, Durham, New Hampshire, USA

Abstract We present the partitioning of integrated energy flux from four tail reconnection events observed by Cluster, focusing on the relative contributions of Poynting flux, electron, H⁺ and O⁺ enthalpy, and kinetic energy flux in the tailward and earthward directions in order to study temporal and spatial features of each event. We further subdivide the Poynting flux into three frequency bands to examine the possible structures and waves that contribute most significantly to the total Poynting flux from the reconnection region. Our results indicate that H⁺ enthalpy flux is often dominant, but O⁺ enthalpy, electron enthalpy, Poynting flux, and H⁺ kinetic energy flux can contribute significant or greater total energy flux depending on spacecraft location with respect to the current sheet, flow direction, temporal scale, and local conditions. We observe integrated H⁺ enthalpy fluxes that differ by factors of 3–4 between satellites, even over ion inertial length scales. We observe strong differences in behavior between H⁺ and O⁺ enthalpy fluxes in all events, highlighting the importance of species-specific energization mechanisms. We find tailward-earthward asymmetry in H⁺ enthalpy flux, possibly indicative of the influence of the closed earthward boundary of the magnetotail system. Frequency filtering of the Poynting flux shows that current sheet surface waves and structures on the timescale of current sheet flapping contribute significantly, while large-scale structure contributions are relatively small. We observe that the direction and behavior of the Poynting flux differs between bands, indicating that the observed flux originates from multiple distinct sources or processes.

1. Introduction

Tail reconnection is considered to be an important driver of geomagnetic activity and aurora at the Earth by allowing magnetic energy stored in field lines to be released into plasma heating, particle acceleration, and electromagnetic waves. The physics of energy outflow from these regions is an area of intense study due to the impact these events have on the magnetosphere, ionosphere, and Earth, as well as the microphysics of particle energization that can be studied in these regions. The fleet of Cluster satellites has had multiple encounters with regions of plasma where reconnection was ongoing. This study will examine two events in 2001 with satellite separations of approximately 2000 km and two events in 2003 with satellite separations of approximately 200 km.

Reconnection event encounters can be identified by consistency with the Walen relation and generally correspond to a magnetic field reversal in B_z , bipolar ion flows, and signatures of Hall fields [Hones, 1976; Sonnerup et al., 1981]. A satellite crossing the ion diffusion region would see a sudden reversal of the magnetic field direction in the geocentric solar ecliptic (GSE) z direction associated with the magnetic field reconfiguration across the X line. In addition, we measure bipolar ion jets tailward and earthward indicating the passage of the X line region over the satellite array. These outflowing jets are decoupled from the motion of the electrons, which are still bound to the magnetic fields and flowing toward the separatrix. This charge separation sets up a Hall current and results in a characteristic quadrupolar magnetic field out of the plane of reconnection (using a simplistic 2-D model for reconnection). The Hall currents and magnetic fields and associated Hall electric fields have been observed in past studies of in situ data [Øieroset et al., 2001; Eastwood et al., 2010; Runov et al., 2003; Wygant et al., 2005; Mozer et al., 2002].

Previous studies on the energy fluxes from reconnection events have utilized in situ satellite data, particle-in-cell (PIC) simulations, hybrid simulations, and lab plasma experiments. A statistical study by *Eastwood et al.* [2013] of Cluster observations of reconnection events indicated that, on average, the outgoing flux is dominated by the proton enthalpy flux which is approximately 2 times greater in the tailward direction than the earthward direction. The next most significant contribution came from the electron enthalpy flux in the tailward direction and the Poynting flux in the earthward direction. In a study utilizing hybrid simulations of symmetric and asymmetric reconnection, *Aunai et al.* [2011] also found that proton enthalpy flux dominated over bulk kinetic energy or proton heat flux and resistive MHD simulations by *Birn and Hesse* [2005] demonstrated that Poynting flux is converted to ion enthalpy flux in large quantities. *Goldman et al.* [2016] also showed with 2-D PIC simulations that ion enthalpy fluxes dominate in the x direction over Poynting flux and ion kinetic energy flux, particularly in the exhaust region.

However, studies of individual events indicate that the contribution of each energy flux to the overall energy budget varies greatly from event to event and on different spatial and temporal scales. Observed energy outflows can be affected by the satellite's proximity to the current sheet [*Nakamura et al.*, 2006; *Birn and Hesse*, 2005], by the plasma conditions [*Wygant et al.*, 2005], or by waves propagating across the plasma sheet [*Dai et al.*, 2011]. Computer simulations have suggested that the relative importance of Poynting flux will vary based on whether or not a guide field is present [*Birn and Hesse*, 2010]. A recent PIC simulation and lab plasma experiment by *Yamada et al.* [2015] also suggests that Poynting flux is a significant or dominant source of energy, along with electron enthalpy flux. In addition, O⁺ contributions have not been separately explored in the Eastwood statistical study, but studies by *Wygant et al.* [2005] and *Kistler et al.* [2005] indicate that it may be an important energy source in some events.

In this study, we will examine the earthward and tailward energy fluxes from four reconnection events in the magnetotail measured by the Cluster satellite fleet. We will focus on the enthalpy flux, and kinetic energy fluxes from electrons, H⁺ ions, and O⁺ ions, and the Poynting flux. We will further filter the Poynting flux into three frequency bands to study what structures or waves contribute to the overall Poynting flux. Of interest in this study are the relative contributions to the overall energy budget of each quantity in the tailward and earthward directions and how these vary over spatial and temporal scales. In order to facilitate this, we have chosen two events that occurred during large spacecraft separation of the Cluster fleet and two events that occurred during small separation.

Section 2 describes the Cluster satellite instruments that provided the data and an overview of the quantities to be calculated. Section 3 provides a detailed description of the plasma conditions during each event, the observed integrated energy fluxes, and notable features. Section 4 presents the observed features of the frequency-filtered Poynting flux. Section 5 discusses the implications of the observations, and section 6 summarizes these findings and suggests future work.

2. Data Sets and Methodology

2.1. Instrumentation

Magnetic field measurements were taken by the fluxgate magnetometer on board each of the four satellites [*Balogh et al.*, 2001]. This instrument consists of two detectors mounted on a 5 m boom in the spacecraft spin plane which measure three-dimensional vector data. These instruments are capable of providing data at 0.1 nT accuracy with temporal resolution of up to 67 vectors per second. In this study, we used only spin resolution (4 s) data due to limits in the electric field measurements.

Electric fields in the plasma were measured using the Electric Field and Wave (EFW) instrument on Cluster [*Gustafsson et al.*, 1997]. This instrument consists of four spherical probes extended on 50 m rotating booms in the spin plane of the satellite. EFW is capable of 2-D vector data at up to 0.1 ms time resolution and 22 $\mu\text{V/m}$ accuracy. However, due to a failure of some of the probes on each satellite, high-resolution data were unavailable. Instead, we used spin resolution data (4 s). In addition, because there are no measurements taken along the spin axis of the satellite (which is approximately aligned to GSE Z), this component of the electric field must be deduced rather than measured. One simple but crude method of handling this ambiguity is to simply assume $E_z = 0$ to remove the missing data. Alternatively, we could reconstruct the full electric field vector using the property that $\mathbf{E} \cdot \mathbf{B} = 0$. This is a reasonable assumption in the MHD regime where parallel electric fields are small. Unfortunately, this reconstruction of the E_z component will result in large errors in the case

where the ratio of $\frac{B_x}{B_z}$ or $\frac{B_y}{B_z}$ are large. To avoid these errors, it is appropriate to remove any data in which these ratios are greater than some threshold value.

In order to avoid large data gaps which would render our integrated fluxes inaccurate, we used $E_z = 0$ as an approximation in this study. However, we performed a preliminary comparison of the total Poynting flux of the reconstructed electric field calculated using $E \cdot B = 0$ in order to estimate the significance of the difference between the two methods. Using a threshold value of 5 for the ratio of $\frac{B_x}{B_z}$ and $\frac{B_y}{B_z}$ and $B_{\text{mag}} \geq 10$ nT and $B_z \geq 2$ nT, we find that the Poynting flux calculated from the two methods differ by less than 30% during the majority of the time span of the events, but significant excursions do occur over short time periods. Over periods of less than 1 min, the Poynting flux calculated using $E \cdot B = 0$ occasionally reached peaks more than 2 times greater than Poynting flux calculated from $E_z = 0$. However, around the time of the X line crossing, Poynting flux calculated from $E \cdot B = 0$ was frequently unavailable due to the thresholds imposed above. This missing data would skew the integrated Poynting flux toward smaller values if used in our analysis below. Furthermore, the strongest Poynting flux peaks may still be inaccurate, even with the thresholds imposed above. We note, therefore, that while using $E_z = 0$ will set a lower limit for *peak* values of the Poynting flux, it will not have a minimizing effect on the *integrated* Poynting flux due to the short time spans of the strong peaks. In fact, due to the amount of data removed by our thresholds, using $E \cdot B = 0$ would cause us to *underestimate* the integrated Poynting flux and is thus inappropriate for our analysis.

Ion data were gathered from the Cluster Ion Spectrometry (CIS) experiment [Rème *et al.*, 1997]. This instrument collects three-dimensional ion distributions with a temporal resolution of 4 s (one spacecraft spin period). The CIS experiment has multiple instruments which measure different energy ranges and species. In particular, in this study we used the Composition and Distribution Function (CODIF) Analyzer instrument which is capable of differentiating between H⁺, He⁺, He⁺⁺, and O⁺ ions with energies below 40 keV. The only species examined here were H⁺ and O⁺, since they are the dominant species in the local plasma. These ion moments were used to calculate the kinetic energy flux and the enthalpy flux for the two different species.

Electron data were gathered from the Cluster plasma electron and current experiment (PEACE) instrument [Johnstone *et al.*, 1997]. This instrument gathers full three-dimensional velocity distributions of electrons with a time resolution of 2 s. In this study, we used the 4 s resolution spin fit data. PEACE is sensitive to energies between 0.59 eV and 26.4 keV. These calculated moments were used to reconstruct the kinetic energy flux and the enthalpy flux for the electrons.

2.2. Calculated Quantities

The primary quantities calculated and discussed in this paper are the Poynting flux and species-specific kinetic energy and enthalpy flux. The Poynting flux describes the amount of energy leaving the reconnection region in the form of electromagnetic waves. The kinetic energy flux describes the energy stored in the bulk motion of the particles. A typical signature of reconnection events are plasma jets—strong, impulsive bursts of plasma flow accelerated in association with the reconfiguration of the magnetic field. The kinetic energy flux describes these jets. Finally, enthalpy flux describes the amount of energy that goes into particle heating via microphysical processes.

The quantities Poynting flux, kinetic energy flux, and enthalpy flux are defined as follows in the x direction:

$$S_x = \frac{(\vec{E} \times \vec{B})_x}{\mu_0} \quad (1)$$

$$K_{s,x} = \left(\frac{1}{2} m_s n_s v_{s,x}^2 \right) v_{s,x} \quad (2)$$

$$H_{s,x} = \frac{\gamma}{\gamma - 1} \text{trace}(\mathbf{P}_s) v_{s,x} \quad (3)$$

Here m is particle mass, v is velocity, n is number density, E and B represent electric and magnetic fields, and P is the pressure tensor. The adiabatic constant γ is taken to be $\frac{5}{3}$. The s subscript indicates species-specific values. Each of these quantities will be calculated in the geocentric solar ecliptic (GSE) coordinate system, wherein GSE x represents the Sun–Earth line and GSE z represents the normal to the ecliptic plane. In this study, we are concerned only with the fluxes in the GSE x coordinate direction, measuring earthward or tailward flow.

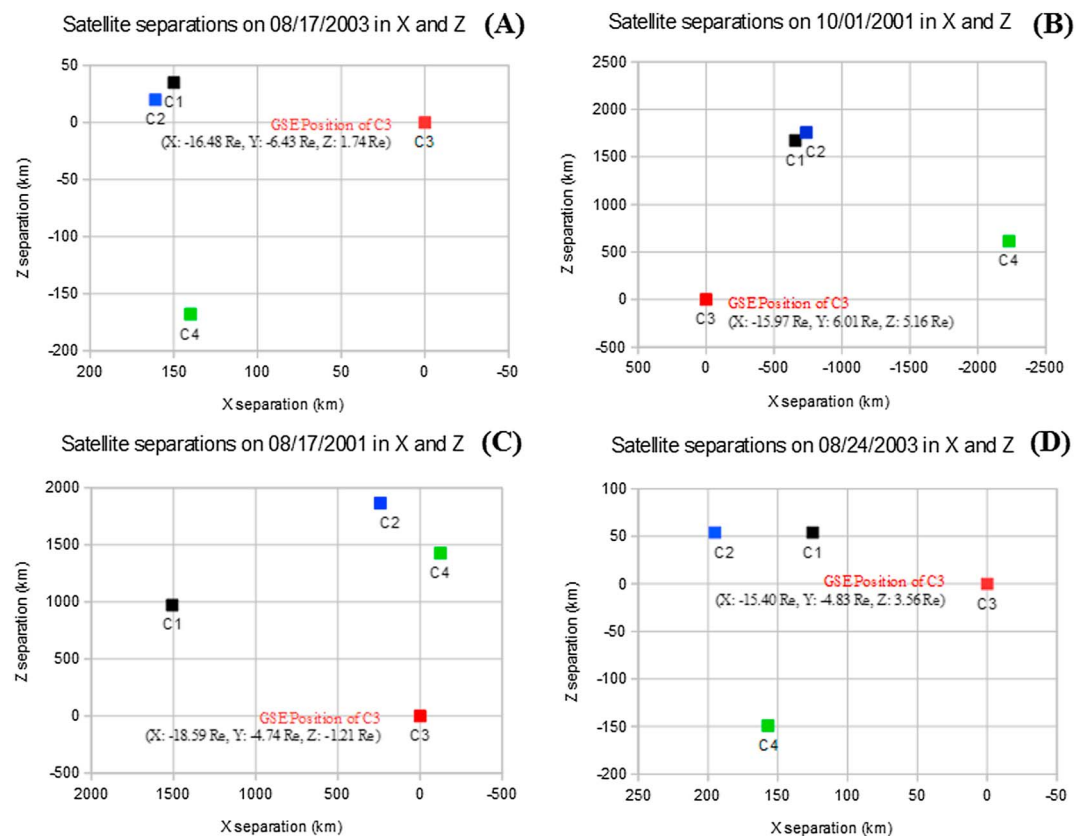


Figure 1. The spatial separations of the Cluster satellites in the GSE X-Z plane for each event. Distances between spacecraft are given in kilometers, with C1, C2, and C4 being plotted relative to the reference spacecraft, C3. (a) Spacecraft separation on 17 August 2003 of about 200 km. (b) Spacecraft separation on 1 October 2001 of about 2000 km. (c) Spacecraft separation on 17 August 2001 of about 2000 km. (d) Spacecraft separation on 24 August 2003 of about 200 km.

The Poynting flux was further analyzed by filtering the data into three frequency bands: 4–60 s, 60–240 s, and 240–600 s. We chose these values due to their correspondence to three distinct features commonly seen in the tail: current sheet surface waves [Dai et al., 2011], current sheet flapping [Sergeev et al., 2003; Runov et al., 2005], and large-scale, quasi-static structures. These frequency bands were calculated by subtracting a running windowed average of the data using an interval equal to the lower frequency limit and then taking a second running windowed average using an interval equal to the upper frequency limit. This process removes low-frequency fluctuations and averages out higher-frequency fluctuations from the data.

For each of the following events, each quantity was calculated and compared in the earthward and tailward direction. In order to quantify the energy partitioning, we integrated the energy fluxes and plotted this integral over time.

3. Event Studies

In this study, we examined two events with large spacecraft separation and two with small spacecraft separation in order to distinguish behaviors over different scales. For reference, in each event, the H⁺ ion inertial length and gyroradius both ranged between approximately 300–600 km. The locations of the satellites during each event are shown in Figure 1. The two events observed in 2001 occurred during a much greater spatial separation of the satellite fleet of the order of multiple ion inertial lengths. Conversely, the events studied in 2003 occurred during a satellite separation of less than an ion inertial length. As a result, the variations in measurements between satellites will be much greater in the 2001 events.

3.1. The 17 August 2003 Event

The first event we will discuss took place on 17 August 2003 between 16:00 and 18:00 UT. This event is a particularly useful baseline as it is the only event in which all of the energy fluxes were able to be measured

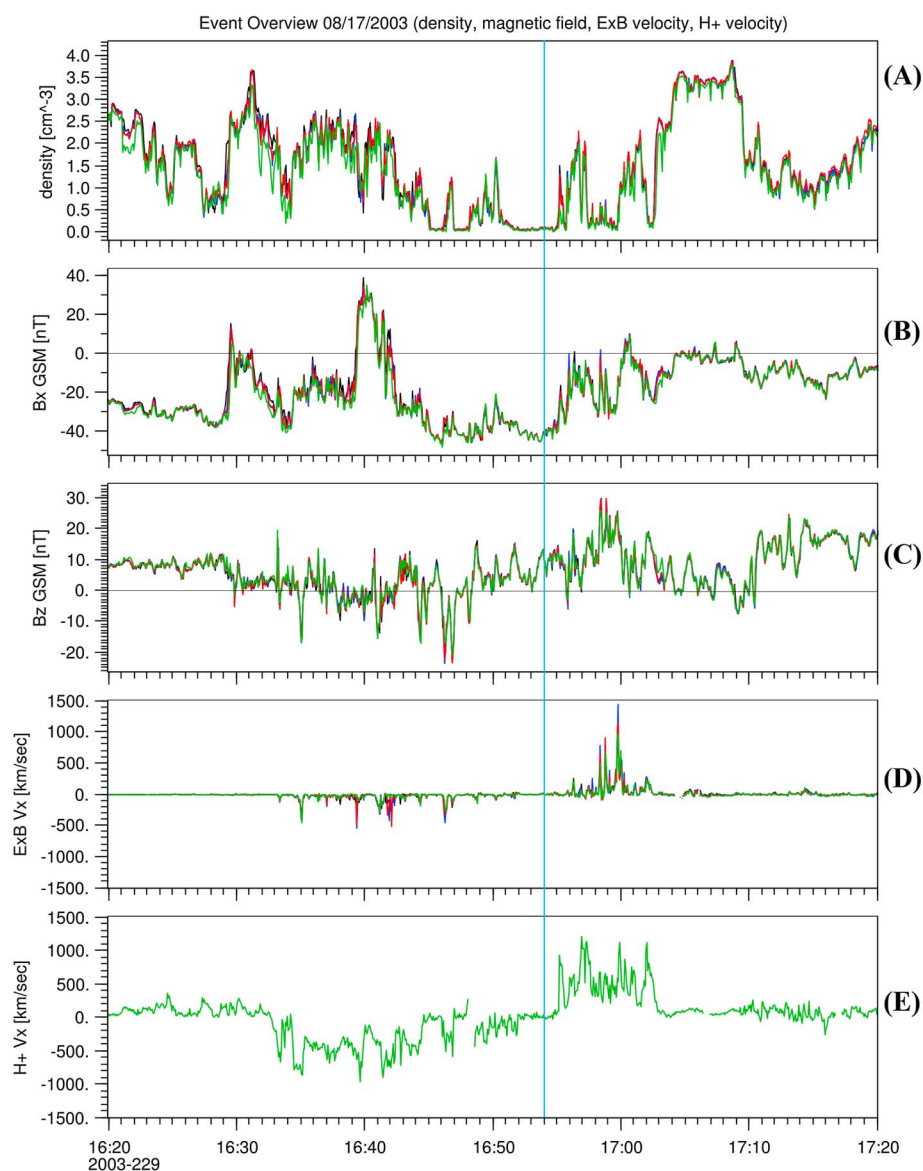


Figure 2. An overview of the reconnection event on 17 August 2003. The panels from top to bottom show (a) the plasma density calculated from spacecraft potential, (b) B_x , (c) B_z , (d) the x component of the ExB velocity, (e) and the x component of the proton velocity. Satellites are plotted in different colors: C1 is black, C2 is blue, C3 is red, and C4 is green. The coordinates used here are Geocentric Solar Magnetic (GSM) coordinates. Although GSE coordinates are used throughout the rest of this paper, GSM coordinates are particularly useful for determining the temporal location of the crossing of the X line, here marked with a vertical blue line.

simultaneously on a single spacecraft (C4). The spacecraft separation was also small at this time, resulting in very similar observations between the spacecraft with no discernible time lag between observed events using the 4 s resolution data.

This event was observed during the precursor to a strong storm that reached its main phase on 18 August 2003. There had been no significant prior geomagnetic activity for approximately 9 days. The Dst at the start of the reconnection event was 25 nT, and the AE index was 265 nT. The Cluster fleet was at 1:12 magnetic local time and approximately 16.5 R_E tailward of Earth. The satellites were separated by a maximum distance of 248 km on the order of an ion inertial length and much greater than an electron inertial length. In this event and all others, Poynting fluxes could be calculated on all four spacecraft. Electron moments were calculated for all spacecraft in this event as well; however, ion moments were only available on Cluster 4. Previous work on this event includes studies of the electric field arising from electron pressure gradients and

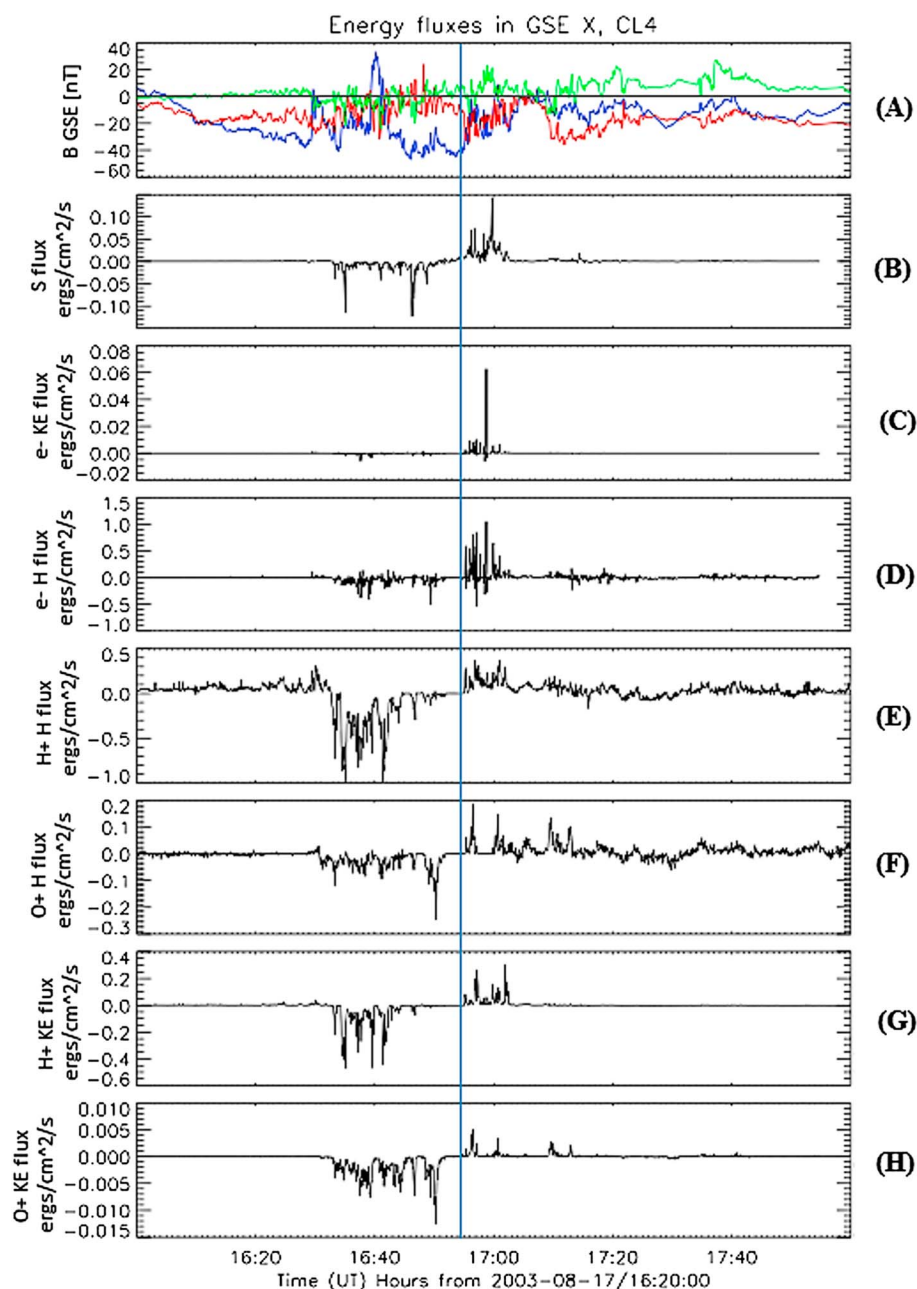


Figure 3. Energy fluxes in GSE X for the event on 17 August 2003 from Cluster 4. From top to bottom: (a) Overlaid magnetic field in GSE X (blue), Y (red), and Z (green); (b) Poynting flux; (c) electron kinetic energy flux; (d) electron enthalpy flux; (e) H⁺ enthalpy flux; (f) O⁺ enthalpy flux; (g) H⁺ kinetic energy flux; and (h) O⁺ kinetic energy flux. All energy fluxes are given in cgs units.

the Hall term [Henderson *et al.*, 2006] and the observation of surface waves on the plasma sheet driven by ion velocity shears [Dai *et al.*, 2011]. This event was included among the events with an observed “flattop” electron energy distribution associated with kinetic acceleration processes [Asano *et al.*, 2008].

Figure 2 is an overview of the plasma conditions during this event. Figure 2a shows the plasma density calculated from the spacecraft potential. Figures 2b and 2c show the magnetic field in geocentric solar magnetic (GSM) coordinates in the X and Z directions, respectively. Figure 2d shows the $E \times B$ velocity calculated in these same coordinates. Finally, Figure 2e shows the H⁺ ion velocity in the X direction. All quantities were plotted from each spacecraft except for the ion velocities which were only available on C4. Due to the small

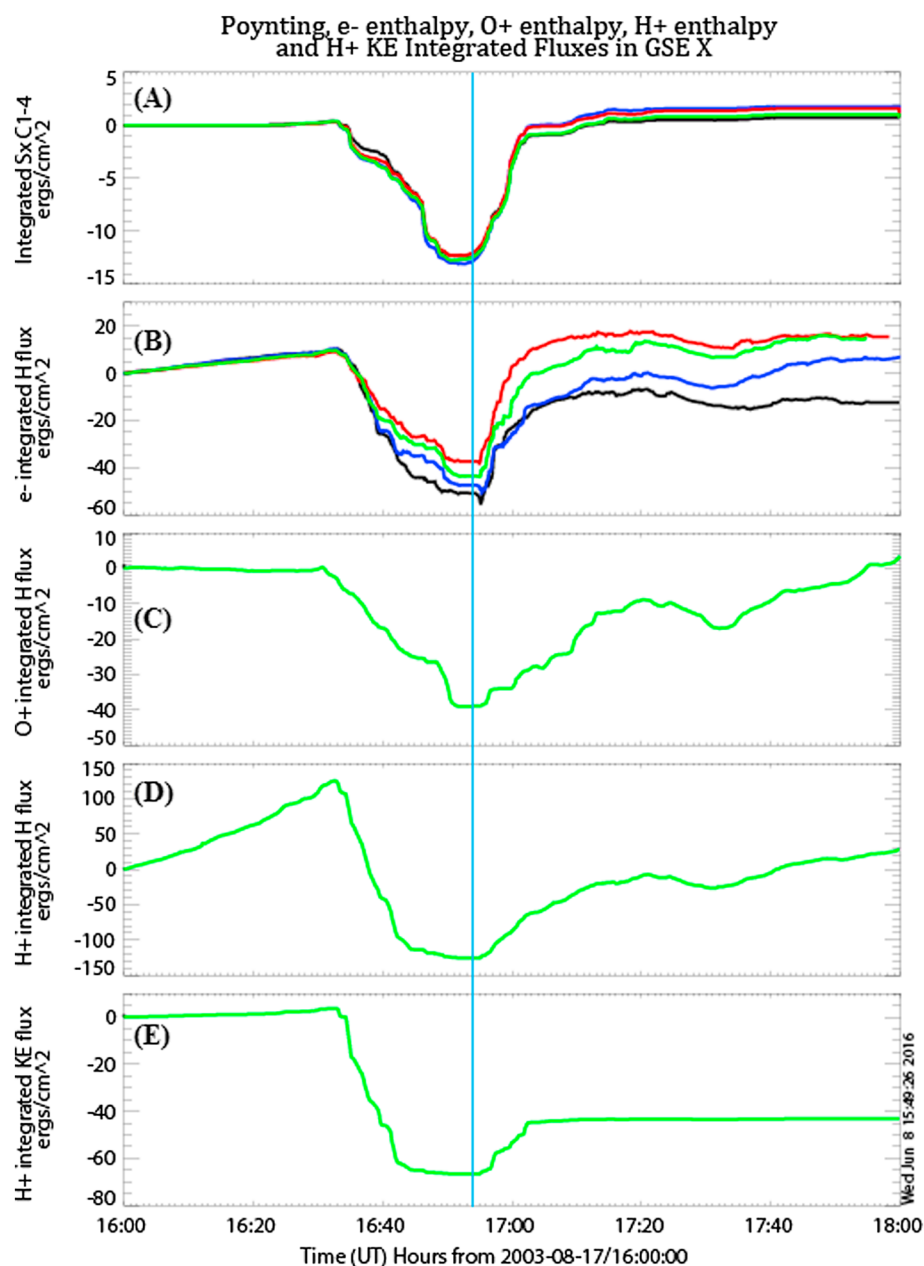


Figure 4. Integrated energy fluxes for the 17 August 2003 event: (a) Poynting flux, (b) e⁻ enthalpy flux, (c) O⁺ enthalpy flux, (d) H⁺ enthalpy flux, and (e) H⁺ kinetic energy flux. Satellites are plotted in different colors: C1 is black, C2 is blue, C3 is red, and C4 is green. The Poynting flux flow is symmetric earthward and tailward, while the ion fluxes are asymmetric with a strong tailward bias. The electron enthalpy is comparable here to the tailward H⁺ KE and the O⁺ enthalpy. The blue vertical line indicates the crossing of the X line.

spacecraft separation, the conditions seen from all satellites appear nearly identical. In this event, the time at which the X line passed above the Cluster spacecraft (marked on Figure 2 by a blue, vertical line) was approximated from the ion velocity and simultaneous $E \times B$ velocity reversal at 16:54 UT. A south-to-north turn of the magnetic field occurs around the same time, but the variability of the B_z component makes it difficult to pinpoint the exact location of this change. On the tailward side of this event we observe at least one crossing of the current sheet, indicated by B_x .

The seven energy fluxes are shown in Figure 3 for the event on 17 August 2003, all from Cluster 4. Figure 3a shows the GSE X, Y, and Z components of the magnetic field in blue, red, and green, respectively. The panels

below display the GSE X component of the Poynting flux (Figure 3b), electron kinetic energy flux (Figure 3c), electron enthalpy flux (Figure 3d), H^+ enthalpy flux (Figure 3e), O^+ enthalpy flux (Figure 3f), H^+ kinetic energy flux (Figure 3g), and O^+ kinetic energy flux (Figure 3h). Tailward energy flux is represented by negative values, while earthward energy flux is represented by positive values. The X line crossing determined above is marked by a vertical blue line.

From Figure 3 we see large peaks in the H^+ enthalpy (especially tailward) and in the electron enthalpy (especially earthward). The ion fluxes remain sustained in the tailward direction over the course of approximately 20 min before a distinct and sustained reversal to the earthward direction. Conversely, the electron enthalpy flux does not remain unidirectional over such long timescales and reverses direction over brief intervals multiple times on both sides of the X line crossing. Although the H^+ enthalpy and electron enthalpy clearly have the largest peak values, contributions from the H^+ kinetic energy flux also appear to be significant. Poynting flux and O^+ enthalpy flux both have relatively minor contributions. The electron and O^+ kinetic energy fluxes are extremely small.

Figure 4 shows five of the largest contributing energy fluxes integrated over time. Figure 4a shows the Poynting flux, Figure 4b the electron enthalpy flux, Figure 4c the O^+ enthalpy flux, Figure 4d the H^+ enthalpy flux, and Figure 4e the H^+ kinetic energy flux. All of the available satellites for each given quantity are plotted in black (C1), blue (C2), red (C3), and green (C4). For this event, Poynting flux and electron measurements were available on all four satellites, but ion measurements were only available on spacecraft 4.

From this figure we can see that the H^+ enthalpy flux in the tailward direction strongly dominates over the other fluxes. The tailward H^+ kinetic energy flux is comparable to the electron enthalpy flux in this direction. However, both H^+ associated fluxes are much weaker in the earthward direction. This leads to the electron enthalpy flux being comparable to the H^+ enthalpy flux in the earthward direction, while the earthward H^+ kinetic energy flux becomes comparatively small. This event occurred following a relatively quiet period of geomagnetic activity, so we do not expect a high density of atmospheric O^+ ions in the magnetosphere. However, the O^+ enthalpy observed in this event is large, comparable in both directions to the e^- enthalpy flux. Unlike the H^+ associated fluxes, the O^+ enthalpy flux does not show a tailward-earthward asymmetry.

This is the only event where the electron enthalpy flux could be measured on all four spacecraft. While some variation is apparent between the four measurements, they each follow a similar pattern of a slow-onset tailward flux followed by a faster-onset earthward flux. Cluster 1 and Cluster 2 see a stronger tailward flow, while Cluster 3 and Cluster 4 observe approximately equal energy fluxes in each direction. Although the spacecraft separation here is relatively small, it is still much greater than an electron inertial length.

The Poynting flux in both directions is small in comparison to the other quantities. In this case, we see that the four satellites measure extremely similar behavior and the total flux in the tailward direction is almost identical to the total flux in the earthward direction. Like the electron enthalpy flux, the Poynting flux exhibits a more gradual-onset tailward flow and a faster-onset earthward flow.

3.2. The 1 October 2001 Event

The second event we examined occurred on 1 October 2001 between 9:00 and 11:00 UT. At the time, the Dst was -148 nT during the main phase of a geomagnetic storm. This storm followed a long period where the Dst remained significantly negative since a storm on 25 September 2001. The AE index during the event fell from 806 to 498 nT, but the hours immediately preceding ranged between 600 and 900 nT, indicating strong geomagnetic activity. The Cluster fleet was at 22:20 magnetic local time and approximately $16 R_E$ tailward of Earth. In contrast to the 17 August 2003 event, this event had a very large satellite separation, up to a maximum distance of 2330 km, on the order of 5–10 ion inertial lengths.

During this event, ion data were only available on Cluster 1 and Cluster 4, while electron moments were available only on Cluster 2. Various features of this event have been studied extensively in other articles, including the current sheet and the magnetic field structure and curvature [Runov *et al.*, 2003], intense electric fields and streaming ion beams [Wygant *et al.*, 2005], and large amplitude solitary waves structures at the edge of the current sheet associated with the reconnection [Cattell *et al.*, 2005]. This event was also included in multiple statistical surveys of Cluster encounters with ion diffusion regions [Eastwood *et al.*, 2013, 2010] and was included among other events in which a flattop electron energy distribution was observed associated with kinetic acceleration processes [Asano *et al.*, 2008].

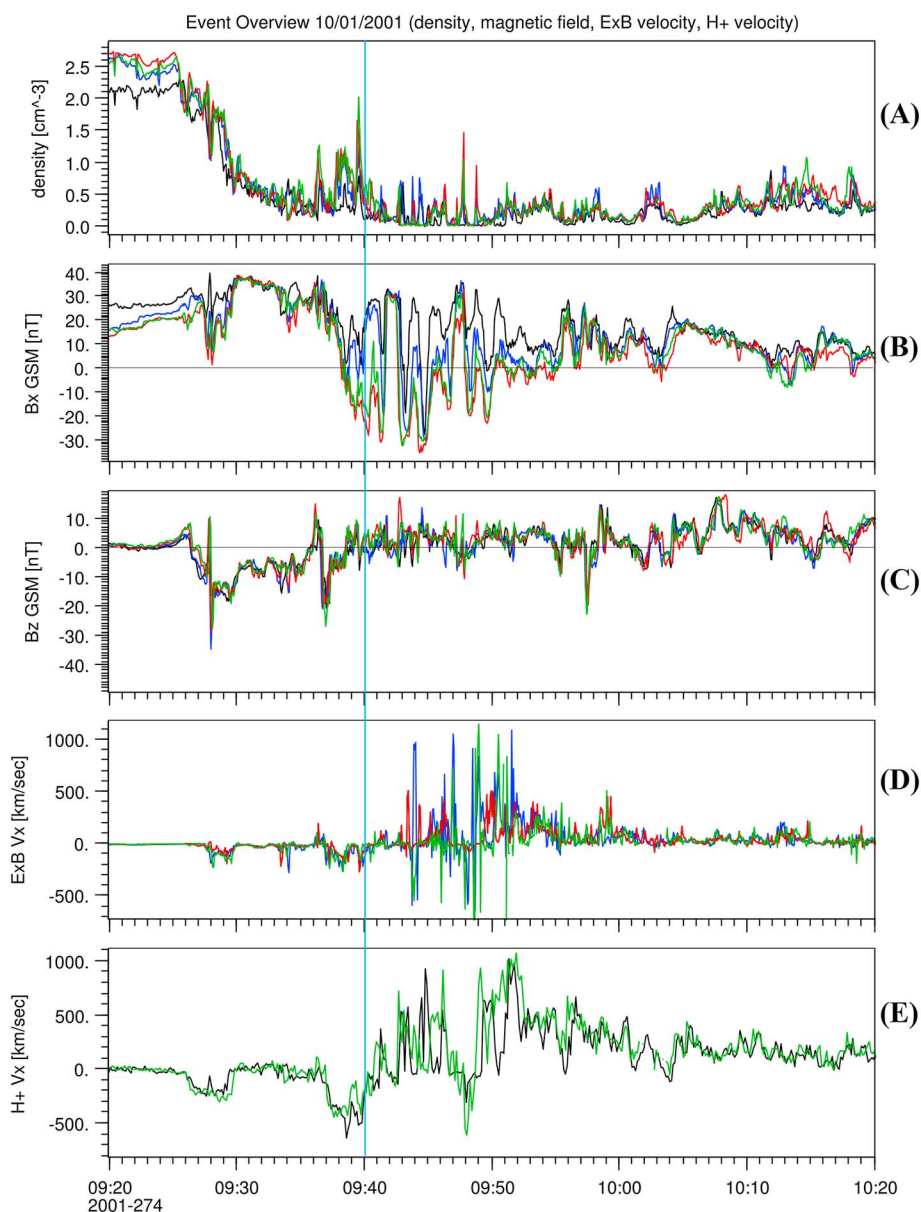


Figure 5. An overview of the reconnection event on 1 October 2001. The panels from top to bottom show (a) the plasma density calculated from spacecraft potential, (b) B_x , (c) B_z , (d) the x component of the $E \times B$ velocity, and (e) the x component of the proton velocity. Satellites are plotted in different colors: C1 is black, C2 is blue, C3 is red, and C4 is green. The coordinates used here are Geocentric Solar Magnetic (GSM) coordinates. Although GSE coordinates are used throughout the rest of this paper, GSM coordinates are particularly useful for determining the temporal location of the crossing of the X line, here marked with a vertical blue line.

Figure 5 shows the plasma conditions at the time of this event on all spacecraft except ion velocities on C1 and C4 only, in the same format as Figure 2. Around 9:40 UT, Clusters 1, 3, and 4 observe B_z change direction, corresponding to a rapid change in ion velocity from tailward to earthward. This is marked as the approximate time of the X line crossing above or below the spacecraft. The x component of the magnetic field changes from positive to negative multiple times after the passage of the X line, indicating multiple crossings of the current sheet. In particular, C2 and C4 observe the most reversals of the magnetic field, while C1 remains primarily above the current sheet, and C3 remains primarily below it.

The seven energy fluxes are shown in Figure 6 for the event on 1 October 2001, all from Cluster 4 with the exception of the electron associated fluxes from Cluster 2. The format is the same as in Figure 3. We observe in the H⁺ and O⁺ fluxes two strong tailward flow regions, while earthward flow is observed to be lesser in

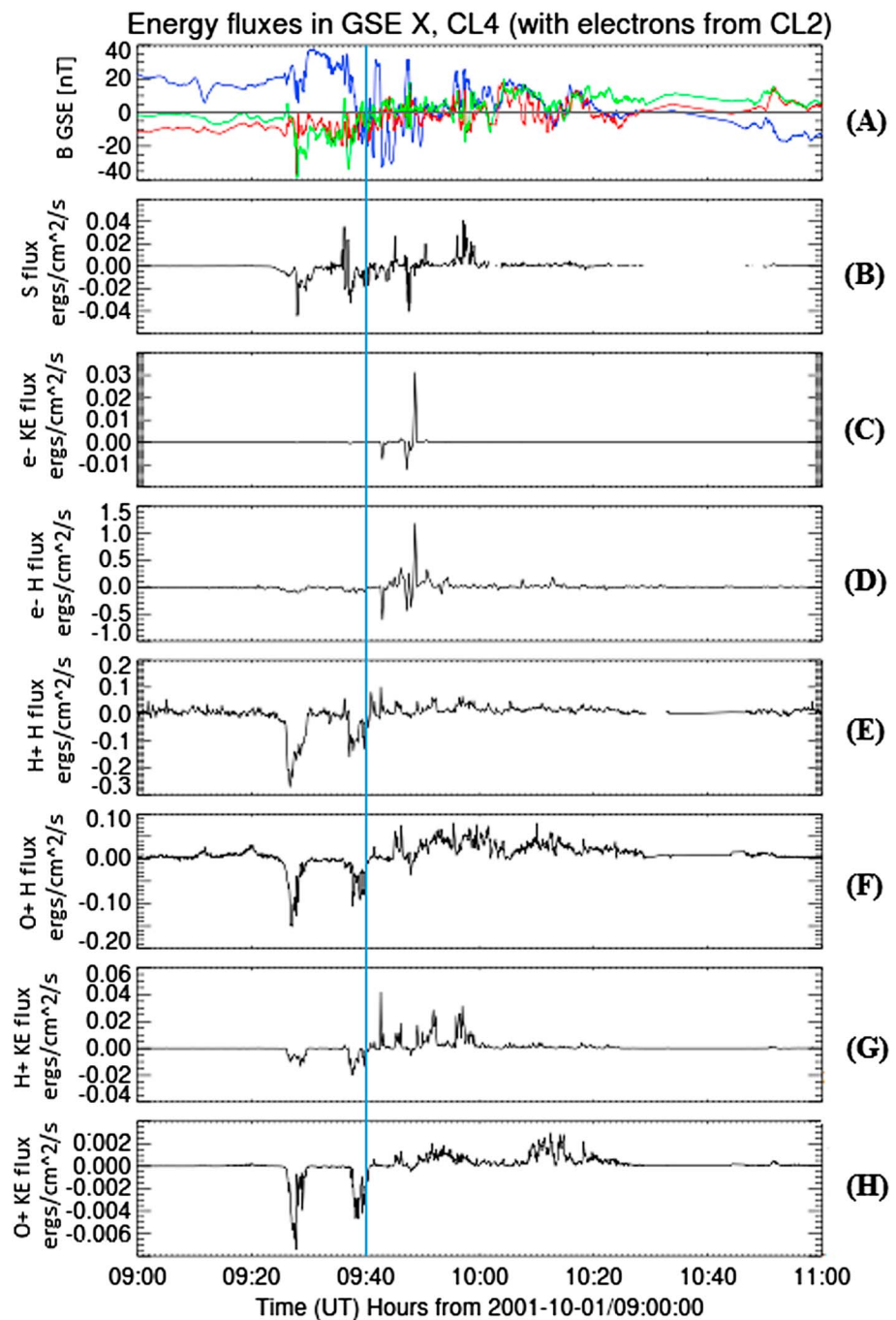


Figure 6. Energy fluxes in GSE X for the event on 1 October 2001 from Cluster 4, with electron measurements from C2. From top to bottom: (a) Overlaid magnetic field in GSE X (blue), Y (red), and Z (green); (b) Poynting flux; (c) electron kinetic energy flux; (d) electron enthalpy flux; (e) H+ enthalpy flux; (f) O+ enthalpy flux; (g) H+ kinetic energy flux; and (h) O+ kinetic energy flux. All energy fluxes are given in cgs units.

magnitude. The electron enthalpy flux is strongly peaked but lasts only for very short intervals. The Poynting flux shows multiple short-term reversals of direction that are not as prominent in the other fluxes, but the peak values are low compared to the electron and ion enthalpy fluxes. The electron and O+ kinetic energy fluxes are very small.

Figure 7 shows five of the largest contributing energy fluxes integrated over time in the same format as Figure 4. We see that H+ enthalpy flux and electron enthalpy flux are both roughly equally dominant in the

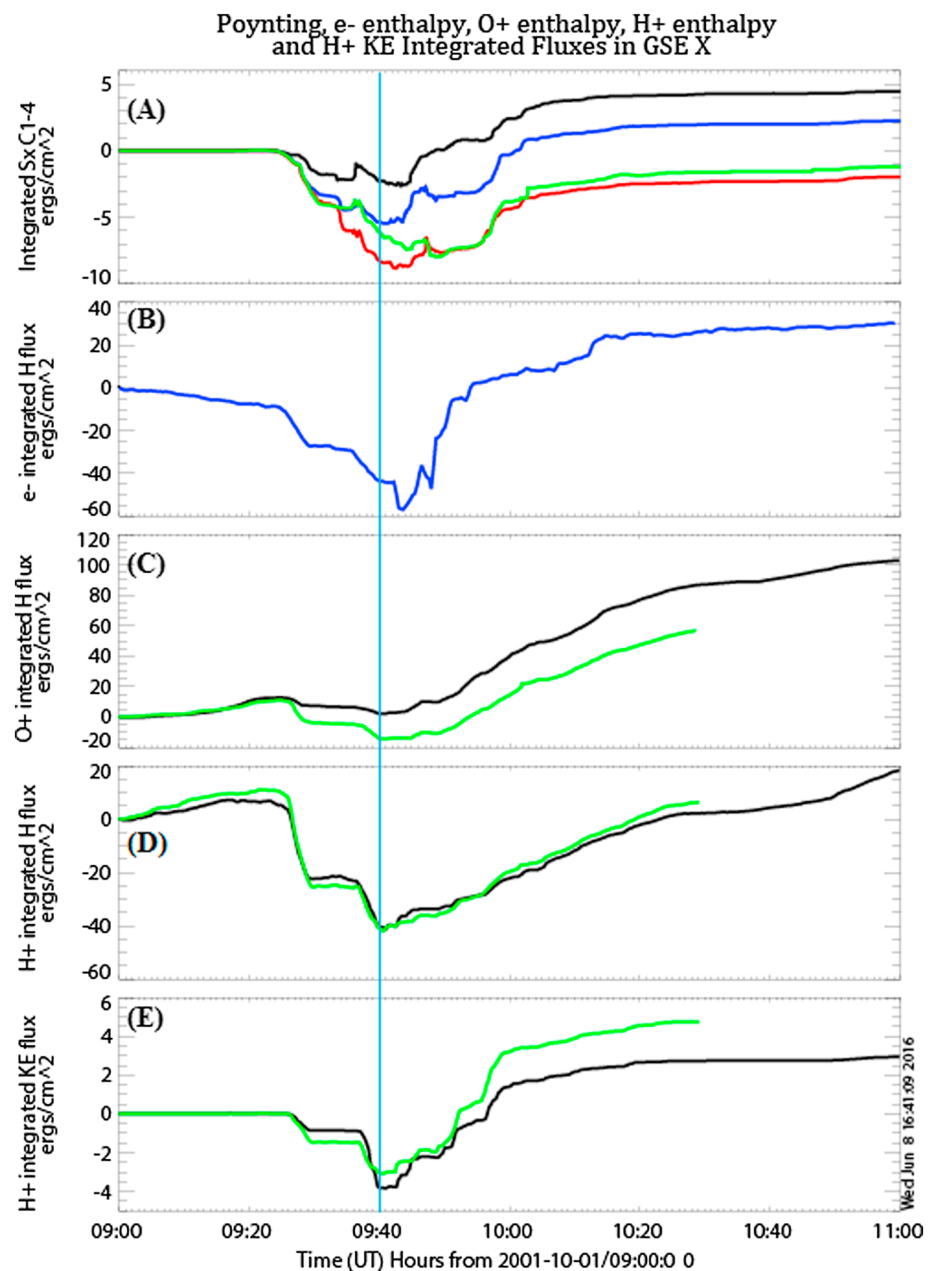


Figure 7. Integrated energy fluxes for the 1 October 2001 event: (a) Poynting flux, (b) e- enthalpy flux, (c) O+ enthalpy flux, (d) H+ enthalpy flux, and (e) H+ kinetic energy flux. Satellites are plotted in different colors: C1 is black, C2 is blue, C3 is red, and C4 is green. Unlike the previous event, the asymmetry in the H+ fluxes is largely absent. The electron enthalpy flux contributes approximately the same amount in both the earthward and tailward directions as the H+ enthalpy flux, while the H+ KE flux is negligible. O+ enthalpy flux in the earthward direction is the dominant energy flux, but there is little O+ enthalpy flux in the tailward direction. The blue vertical line indicates the crossing of the X line.

tailward direction, while O+ enthalpy flux strongly dominates in the earthward direction. Poynting flux and H+ kinetic energy flux contribute an insignificant amount to the overall energy flux. Figure 7d shows a very rapid onset of the tailward H+ enthalpy flux compared to a more gradual onset of Poynting flux and electron enthalpy flux in Figures 7a and 7b. For the H+ enthalpy flux, the greatest contribution occurs early in the event in contrast to the other fluxes.

Due to the large spacecraft separation, we expected to see significant variation between the fluxes measured on each spacecraft. The Poynting flux is notably less symmetric than in the previous event and with

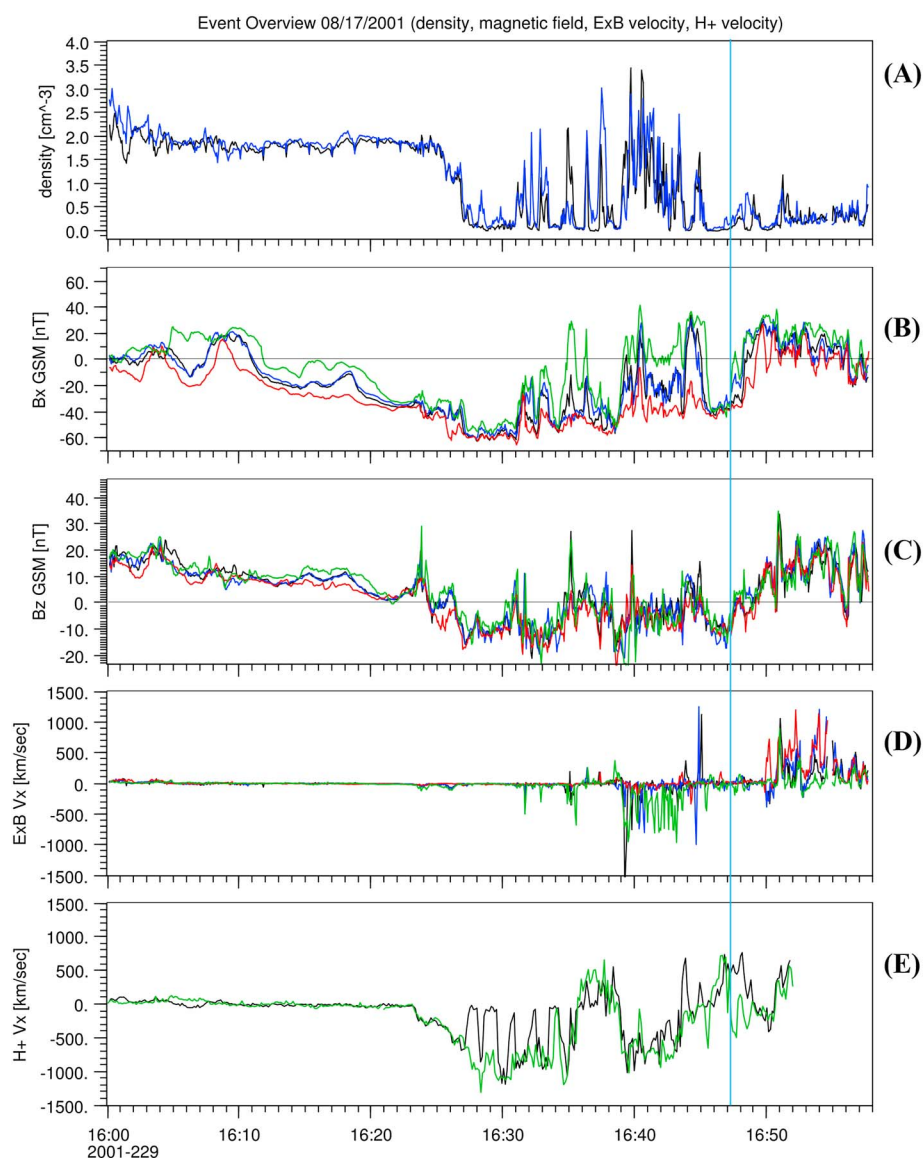


Figure 8. An overview of the reconnection event on 17 August 2001. The panels from top to bottom show (a) the plasma density calculated from spacecraft potential, (b) B_x , (c) B_z , (d) the x component of the $E \times B$ velocity, and (e) the x component of the proton velocity. Satellites are plotted in different colors: C1 is black, C2 is blue, C3 is red, and C4 is green. The coordinates used here are Geocentric Solar Magnetic (GSM) coordinates. Although GSE coordinates are used throughout the rest of this paper, GSM coordinates are particularly useful for determining the temporal location of the crossing of the X line, here marked with a vertical blue line.

significant variation between the spacecraft. Particularly, the earthward flux is almost identical on each spacecraft, but the tailward flux is minimal on C1 and maximal on C3. However, the H^+ enthalpy flux is very similar between C1 and C4, even though C4 was likely closer to the plasma sheet based on density and magnetic field measurements in Figure 5. In addition, unlike the previous event, there does not seem to be a strong earthward-tailward asymmetry in the H^+ fluxes. In fact, for the H^+ enthalpy and kinetic energy, the flux in each direction are very nearly equal although the tailward flow occurs over much shorter timescales than the earthward flow. C4 observes more earthward kinetic energy flux than C1 does, likely because C4 is often in a higher-density regime close the plasma sheet.

Unlike the H^+ fluxes, the O^+ enthalpy flux shows a strong preference toward earthward flux on both C1 and C4. In fact, C1 sees almost no tailward O^+ enthalpy flux at all. The spacecraft separation at this time is of the order of a few oxygen inertial lengths.

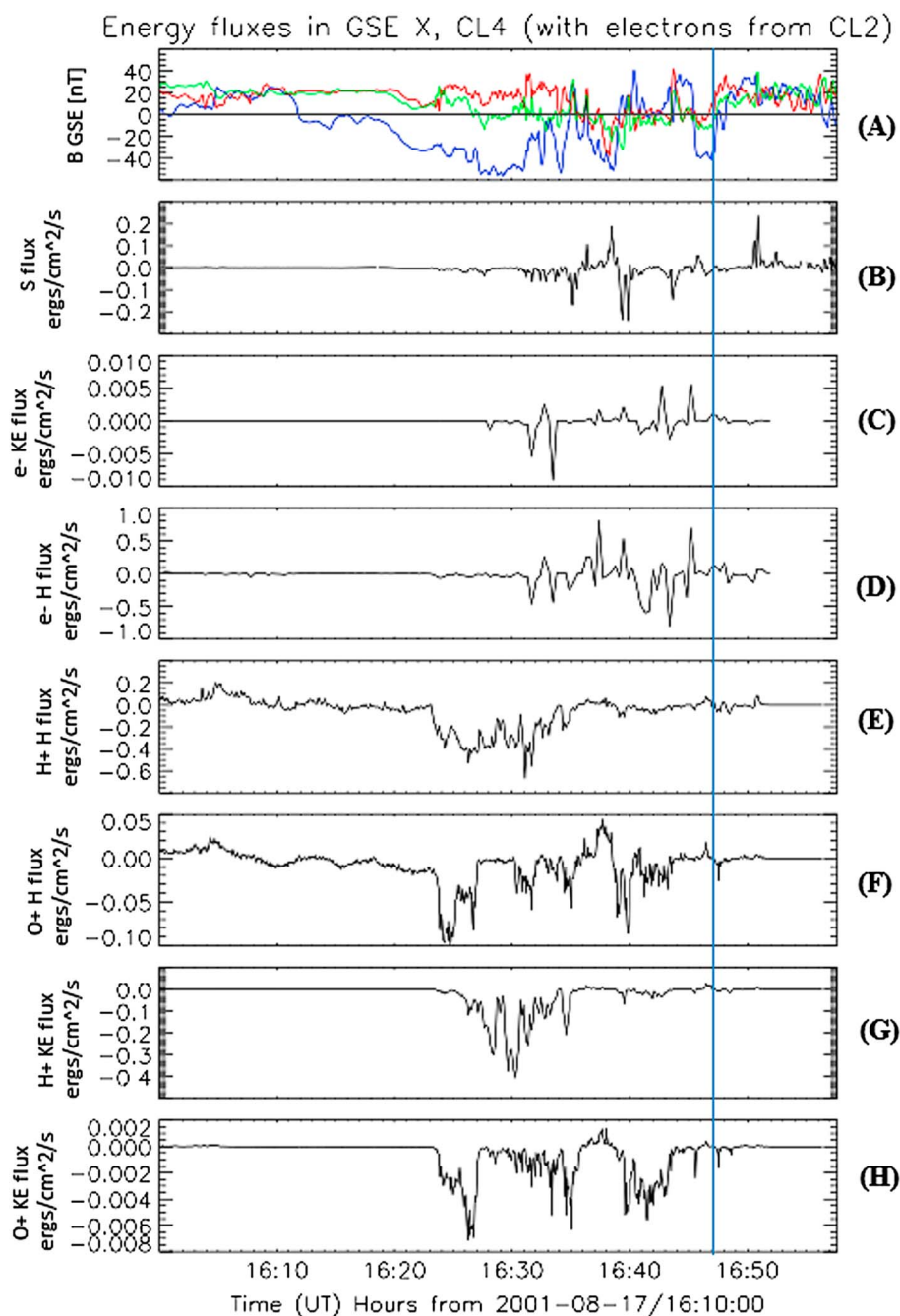


Figure 9. Energy fluxes in GSE X for the event on 17 August 2001 from Cluster 4, with electron measurements from C2. From top to bottom: (a) Overlaid magnetic field in GSE X (blue), Y (red), and Z (green); (b) Poynting flux, (c) electron kinetic energy flux, (d) electron enthalpy flux, (e) H⁺ enthalpy flux, (f) O⁺ enthalpy flux, (g) H⁺ kinetic energy flux, and (h) O⁺ kinetic energy flux. All energy fluxes are given in cgs units.

3.3. The 17 August 2001 Event

The third event that we studied occurred on 17 August 2001 between 16:00 and 17:00 UT. At the time, the *Dst* was 16 nT during a precursor to a geomagnetic storm that reached a minimum of −105 nT later that day. Geomagnetic activity was high, with *AE* ranging from 875 to 1106 nT during the course of the event. The Cluster fleet was at 1:06 magnetic local time and approximately 18.5 R_E tailward of the Earth. Similar to the previous event, the satellites were separated by a maximum distance of 2000 km, on the order of several ion inertial lengths. Ion moments were only available at this time on Cluster 1 and 4, while electron moments were available only on Cluster 2. Furthermore, all satellite data were unavailable after 16:52 UT, unfortunately

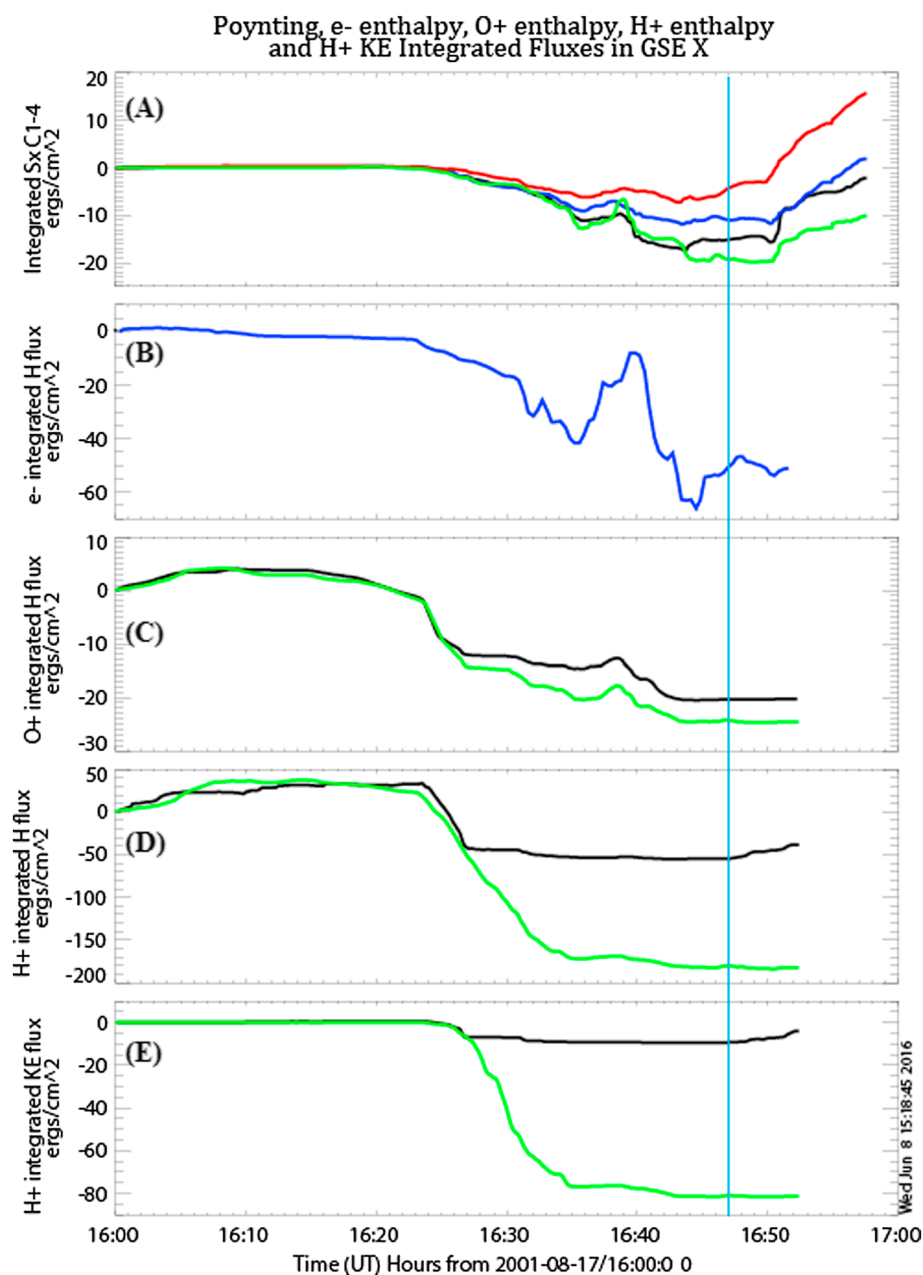


Figure 10. Integrated energy fluxes for the 17 August 2001 event: (a) Poynting flux, (b) e⁻ enthalpy flux, (c) O⁺ enthalpy flux, (d) H⁺ enthalpy flux, and (e) H⁺ kinetic energy flux. Satellites are plotted in different colors: C1 is black, C2 is blue, C3 is red, and C4 is green. Notably, there is a large discrepancy between C1 and C4 H⁺ fluxes, although both show a strong tailward-to-earthward asymmetry. The e⁻ enthalpy flux manifests a strong earthward feature before the crossing of the X line that is not observed in any of the other significant fluxes. The Poynting flux is the only energy flux that shows any significant earthward flow, but, because of the missing data, we cannot know if the lack of earthward flows persisted. The blue vertical line indicates the crossing of the X line.

cropping out the majority of the data that could have been collected once the satellites were on the earthward side of the X line. This event was included in a statistical study of 18 ion diffusion region crossings in which a flat-top electron energy distribution was observed associated with kinetic acceleration processes [Asano *et al.*, 2008]. The intense Poynting flux from this event was also associated with an intense electron-driven auroral emission spot above the auroral oval [Cattell *et al.*, 2011].

Figure 8 shows the plasma conditions at the time of this event in the same format as Figure 2. The densities from spacecraft potential were inaccurate for spacecraft 3 and 4 and so were not plotted in Figure 8a,

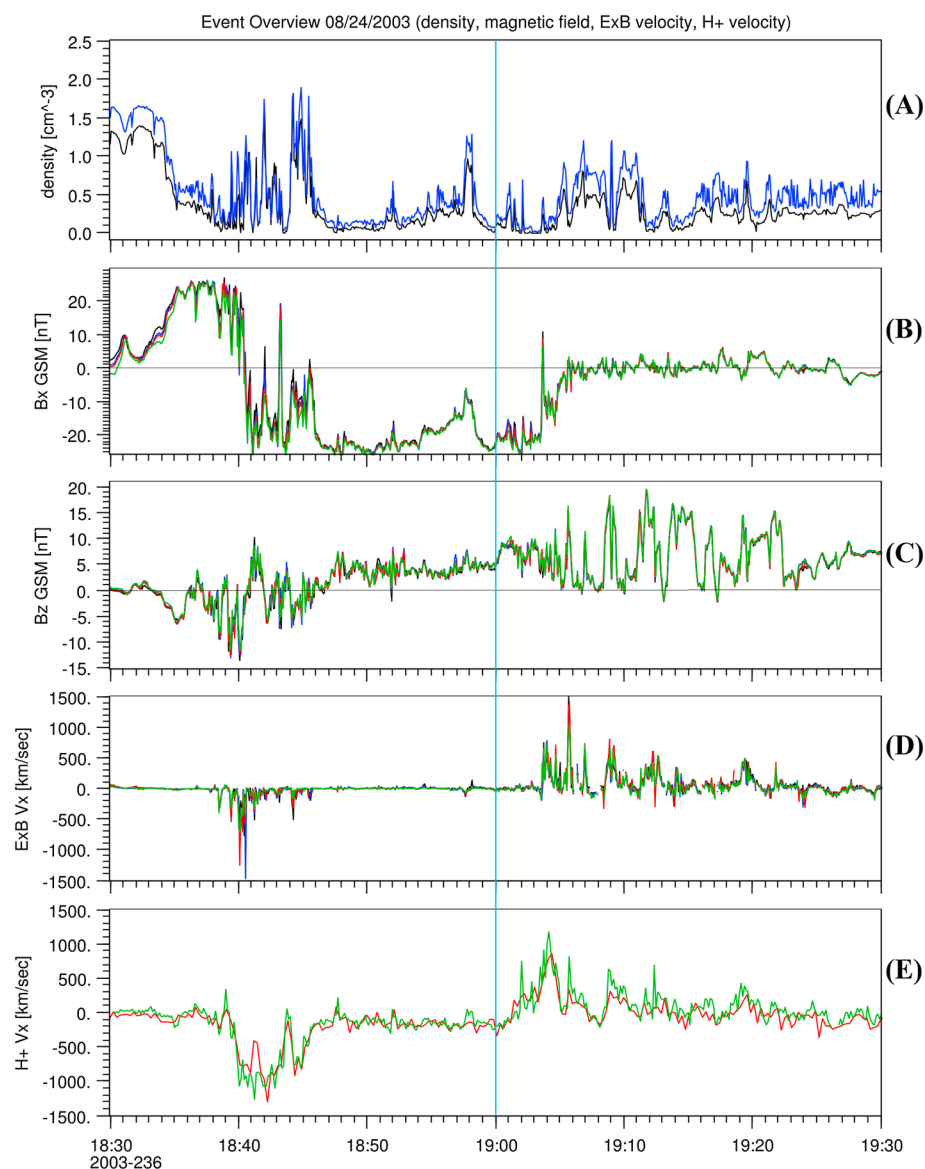


Figure 11. An overview of the reconnection event on 24 August 2003. The panels from top to bottom show (a) the plasma density calculated from spacecraft potential, (b) B_x , (c) B_z , (d) the x component of the $E \times B$ velocity, and (e) the x component of the proton velocity. Satellites are plotted in different colors: C1 is black, C2 is blue, C3 is red, and C4 is green. The coordinates used here are Geocentric Solar Magnetic (GSM) coordinates. Although GSE coordinates are used throughout the rest of this paper, GSM coordinates are particularly useful for determining the temporal location of the crossing of the X line, here marked with a vertical blue line.

while ion velocities were unavailable on spacecraft 2 and 3 and so were not plotted in Figure 8e. Strong tailward ion velocities are seen around 16:23 UT, not associated with strong $E \times B$ velocities. This is followed a few minutes later at 16:26 UT by B_z turning negative and a sudden drop in the density. The x magnetic field fluctuates between negative and positive values 4 times within the span of the data, indicating multiple crossings of the current sheet likely due to flapping. The B_z component of the field also briefly changes direction at least three times until, around 16:47 UT, the B_z magnetic field and x direction ion velocities turn more permanently and strongly positive. We marked this point as the approximate tailward passage of the X line above the spacecraft. Unfortunately, only a few minutes of data remain for this event, so the region in which the satellites lie earthward of the X line cannot be well studied.

The seven energy fluxes are shown in Figure 9 for the event on 17 August 2001, all from Cluster 4 with the exception of the electron associated fluxes from Cluster 2. In this event, we see significant tailward H⁺ and O⁺

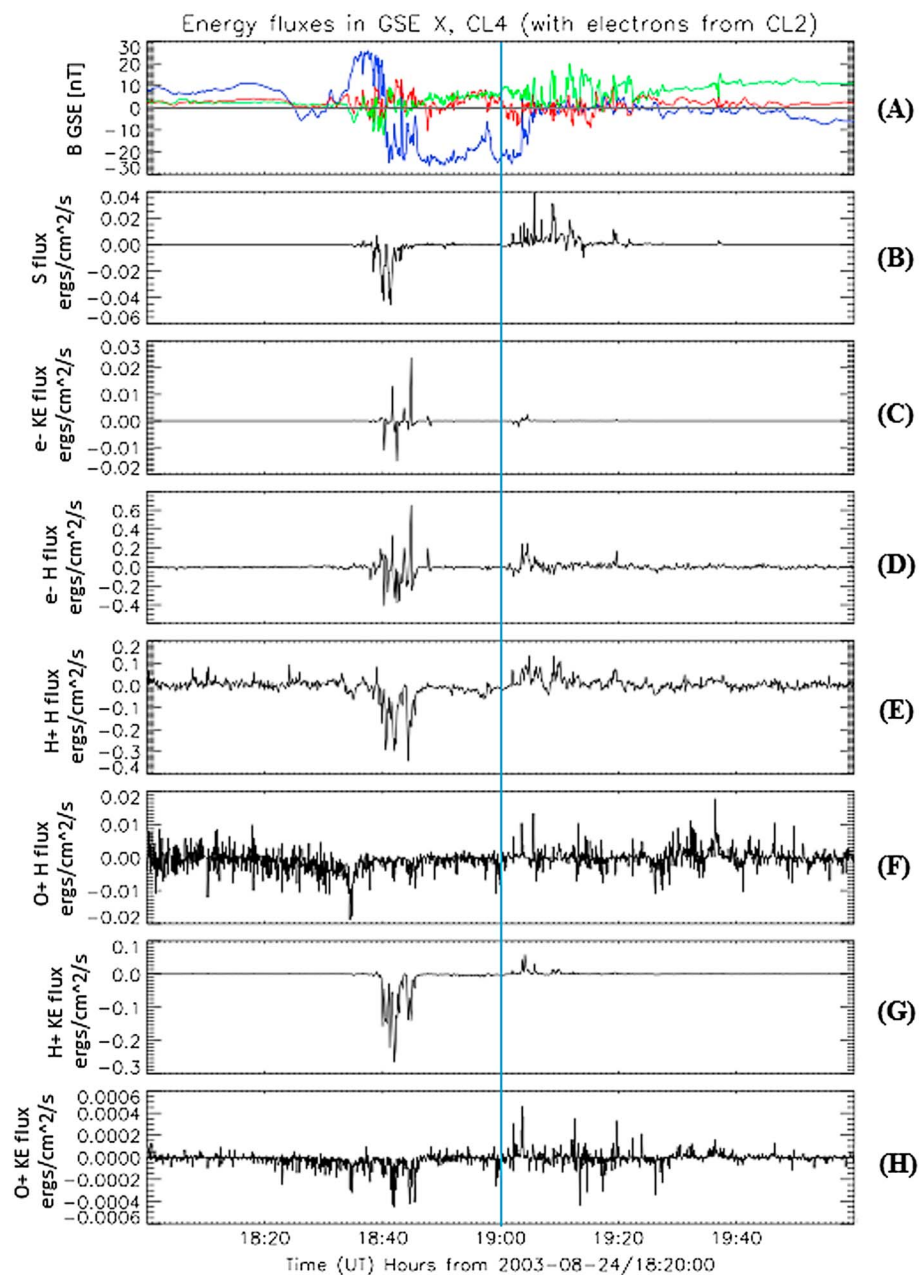


Figure 12. Energy fluxes in GSE X for the event on 17 August 2001 from Cluster 4, with electron measurements from C2. From top to bottom: (a) Overlaid magnetic field in GSE X (blue), Y (red), and Z (green); (b) Poynting flux; (c) electron kinetic energy flux; (d) electron enthalpy flux; (e) H⁺ enthalpy flux; (f) O⁺ enthalpy flux; (g) H⁺ kinetic energy flux; and (h) O⁺ kinetic energy flux. All energy fluxes are given in cgs units.

enthalpy fluxes prior to any significant Poynting or electron associated energy fluxes. For all fluxes, multiple flow reversals were observed indicating that this event might involve multiple reconnection regions. The peak energy fluxes in the ions were much stronger tailward than earthward, while strong peaks in the electron enthalpy were approximately equal in both directions. The Poynting flux also demonstrates roughly equal peaks in both directions. The electron and O⁺ kinetic energy fluxes were negligible in this event.

Figure 10 shows five of the largest contributing energy fluxes integrated over time in the same format as Figure 4. We see that the tailward energy flux is dominated by the H⁺ enthalpy flux. The tailward ion enthalpy and kinetic energy fluxes increase steeply before the satellites observe the negative turning of the B_z magnetic

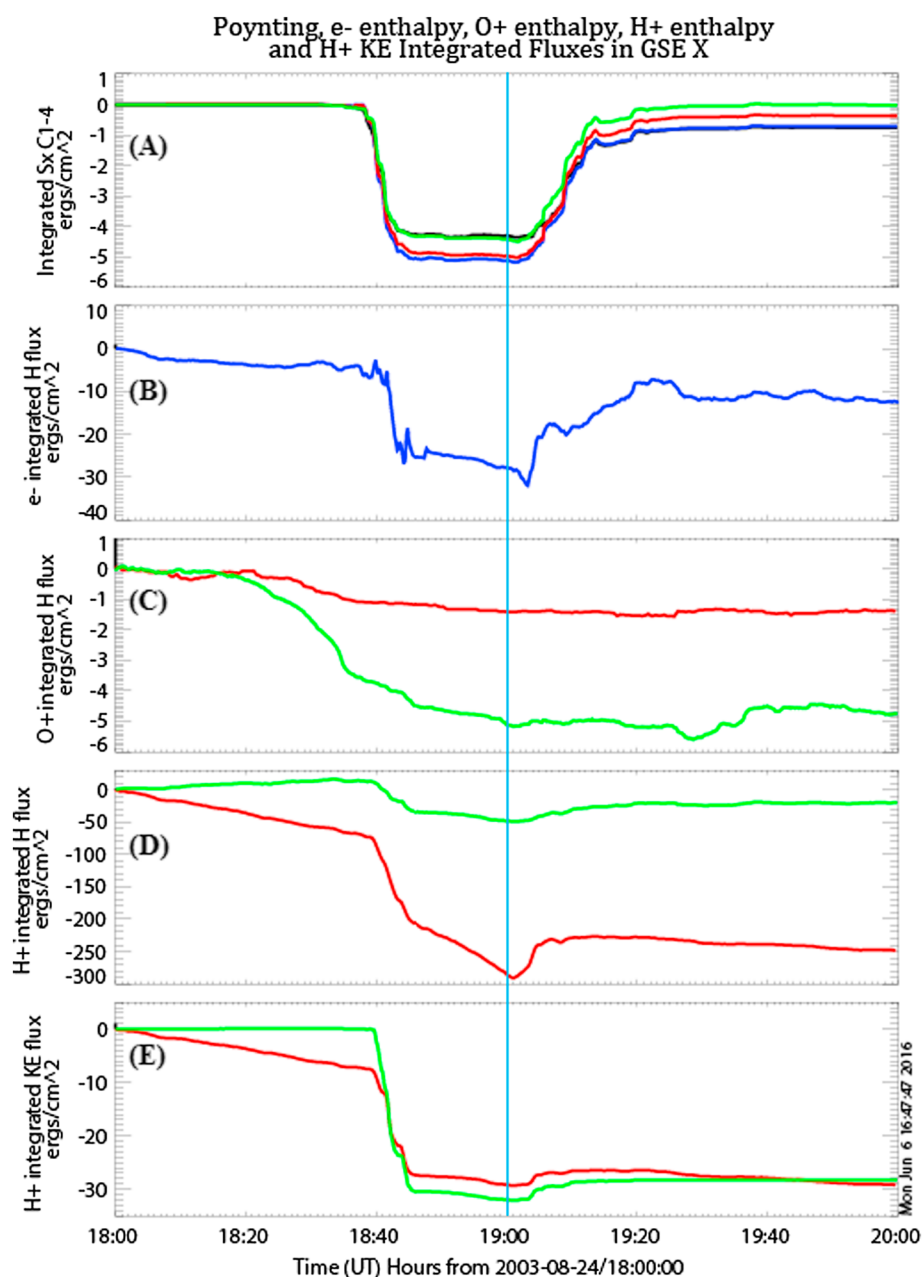


Figure 13. Integrated energy fluxes for the 24 August 2003 event: (a) Poynting flux, (b) e⁻ enthalpy flux, (c) O⁺ enthalpy flux, (d) H⁺ enthalpy flux, and (e) H⁺ kinetic energy flux. Satellites are plotted in different colors: C1 is black, C2 is blue, C3 is red, and C4 is green. Notably, C1 observes much greater tailward H⁺ enthalpy flux than C4 although both show a strong tailward-earthward asymmetry. For the O⁺ enthalpy flux, this is reversed and C4 observes much more than C3. The H⁺ KE flux is nearly identical on both satellites. The Poynting flux is again very symmetric across the X line as is the electron enthalpy flux. The blue vertical line indicates the crossing of the X line.

field (see Figure 8) and before the onset of significant electron-associated energy flows or Poynting flux. As in previous events, the Poynting flux and electron enthalpy flux have a slower tailward onset than the ion fluxes. The electron enthalpy flux also shows a unique strong earthward flow structure prior to the X line crossing that does not seem to correspond to any behavior in the other energy fluxes.

Figures 10d and 10e show a large disparity between the total integrated H⁺ enthalpy and kinetic energy fluxes seen on spacecraft 1 and 4. Cluster 4 observes much greater total ion energy fluxes in the tailward direction. This behavior is not observed in the Poynting flux or O⁺ enthalpy flux.

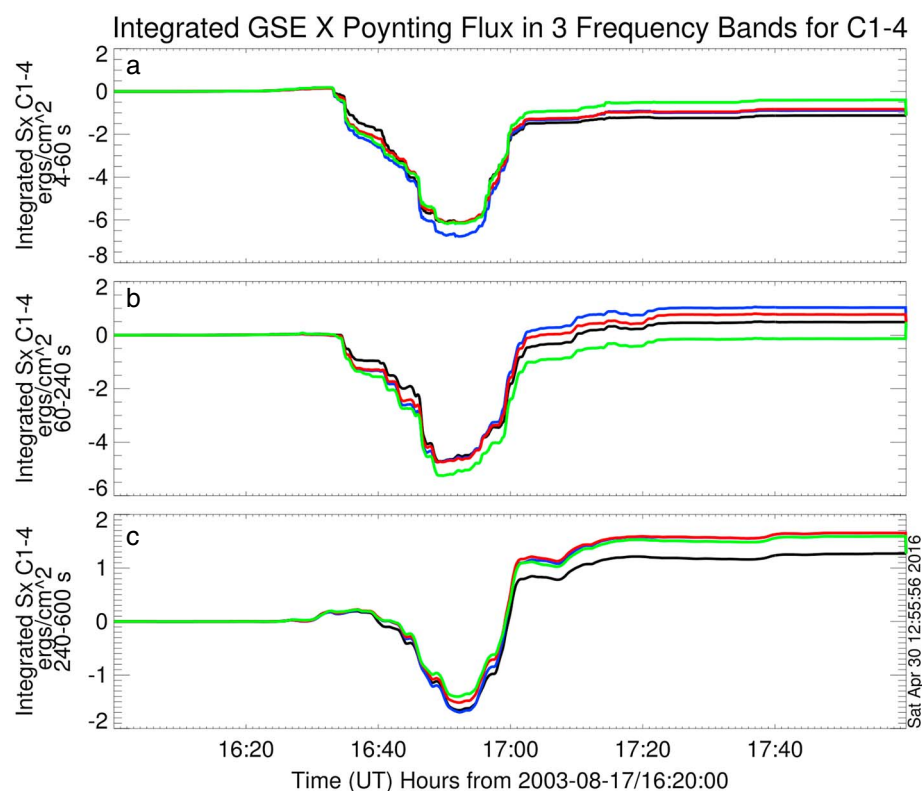


Figure 14. Integrated Poynting flux from 17 August 2003 divided into 4–60 s, 60–240 s, and 240–600 s bands. Spacecraft are distinguished by color (C1 = black, C2 = blue, C3 = red, and C4 = green). The small separation of the satellites is apparent here due to the similarity of each satellite's observations. Notably, the high-frequency band shows greater tailward flux, while the low-frequency band shows greater earthward flux, and the midfrequency band does not show a clear directional preference.

Both Cluster 1 and Cluster 4 observe a tailward-earthward asymmetry in the ion-associated fluxes similar to what was observed in the 17 August 2003 event. Unfortunately, because of operational reasons, there are insufficient data after the passage of the X line to be certain of the persistence of this asymmetry. We do see that the Poynting flux on satellites 1, 3, and 4 has clearly turned strongly earthward before the loss of ion data, suggesting that the observed asymmetry may be real. However, it is inconclusive how significant the asymmetry is due to the missing data.

In this event, the oxygen enthalpy flux is small compared to the H⁺ ion fluxes and electron enthalpy flux and does not contribute significantly to the overall energy flux. However, the behavior of the oxygen ions is significantly different than that of the hydrogen ions. Figure 10c shows that the integrated O⁺ enthalpy flux is approximately equal on C1 and C4, while Figure 10d shows that C4 observes approximately 4 times as much energy flux over time as C1. This is due to the different scales over which O⁺ is energized due to its larger gyroradius.

3.4. The 24 August 2003 Event

The final event addressed in this paper took place on 24 August 2003 between 18:00 and 20:00 UT. At the time, the *Dst* was –29 nT during a long recovery from the –148 nT storm on 18 August 2003. The *AE* reached a maximum value of 730 nT during the event but was only around 100–200 nT in the hours directly before. The Cluster fleet was around 00:45 magnetic local time and approximately 15.6 *R_E* tailward of Earth. The satellites were separated by a maximum distance of 257 km on the order of an ion inertial length and much greater than an electron inertial length. Ion data were only available at this time from Cluster 3 and 4, and electron moments were available only on Cluster 2. This event was identified as an ion diffusion region crossing by Nakamura *et al.* [2006] where the current sheet width and features were measured.

Figure 11 shows the plasma conditions at the time of this event in the same format as Figure 2. The density from spacecraft potential was inaccurate for spacecraft 3 and 4 and so are not plotted in Figure 11a,

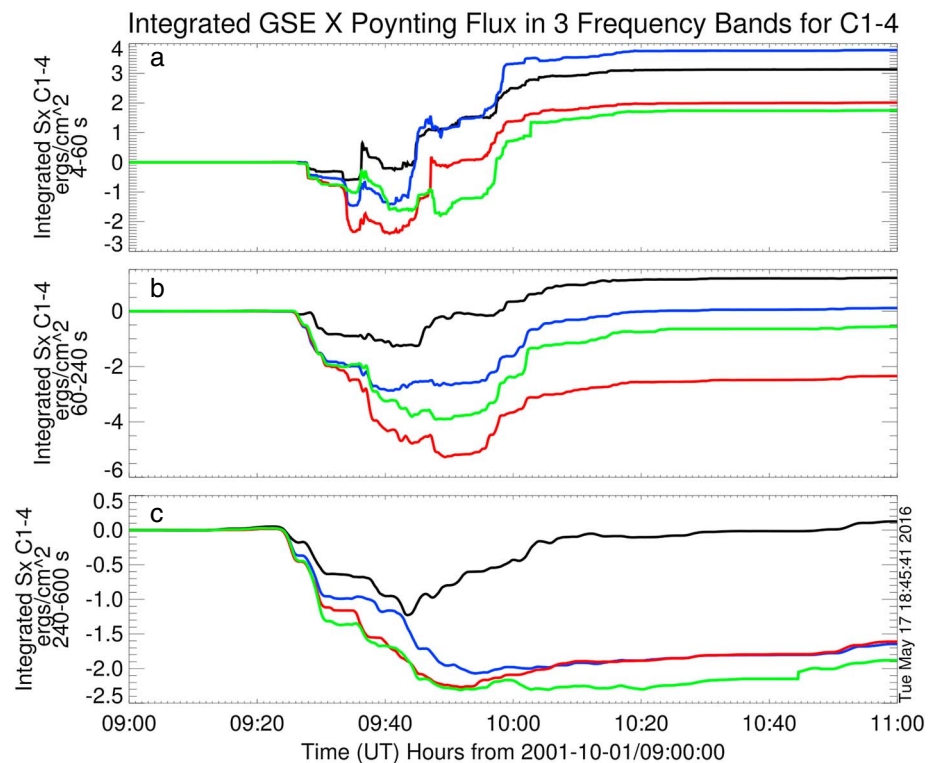


Figure 15. Integrated Poynting flux from 1 October 2001 divided into 4–60 s, 60–240 s, and 240–600 s bands. Spacecraft are distinguished by color (C1 = black, C2 = blue, C3 = red, and C4 = green). In general, the high-frequency band has greater earthward flux, while the low-frequency band shows primarily tailward flux. The tailward flux is dominated by the midfrequency band, while the earthward flux is dominated by high-frequency waves.

while ion velocities were unavailable on spacecraft 1 and 2 and so are not plotted in Figure 11e. In this event, the X line crossing is highly ambiguous, as there is a long interval between 18:47 and 19:02 where the ion and $E \times B$ velocities were nearly zero. The sign of B_z reverses around 18:47 UT but remains at values around 5 nT, making the direction change rather insignificant and an inadequate marker, by itself, of the X line passing above the spacecraft. However, we see in Figure 13 below that the integrated electron enthalpy flux and ion enthalpy flux both are distinctly tailward until around 19:00, so we place the X line crossing approximation at this point.

The seven energy fluxes are shown in Figure 12 for the event on 24 August 2003, all from Cluster 4 with the exception of the electron associated fluxes from Cluster 2. In this event, the H⁺ enthalpy and kinetic energy flows are clearly bipolar, while the electron enthalpy reverses direction multiple times while the satellites are tailward of the X line. The kinetic energy and enthalpy flux for H⁺ have very similar peak values, unlike previous events. The Poynting flux and O⁺ enthalpy flux have very insignificant values, along with the electron and O⁺ enthalpy fluxes.

Figure 13 shows five of the largest contributing energy fluxes integrated over time in the same format as Figure 4. We see in Figure 13d an enormous variation in the H⁺ enthalpy flux between satellites. This is surprising since the satellite separation here is small, roughly on the order of 1 ion inertial length. However, C3 sees a gradual tailward onset of H⁺ enthalpy flux starting long before the other fluxes are seen, and it continues to see a stronger tailward surge for at least 15 more minutes. C4 sees only one short tailward burst, similar to what is observed in the Poynting flux. We note that the H⁺ kinetic energy flux does not show this discrepancy, indicating that C3 is observing only an ion heating event and not an acceleration of bulk plasma motion.

All H⁺ associated fluxes are stronger in the tailward direction than the earthward direction as in both 2001 events, and this behavior is also observed in the O⁺ enthalpy flux. In contrast, the electron enthalpy and Poynting fluxes are very symmetric. The contribution from Poynting flux in both directions and H⁺ kinetic energy flux in the earthward direction are both very small. The contribution from O⁺ enthalpy flux is also very

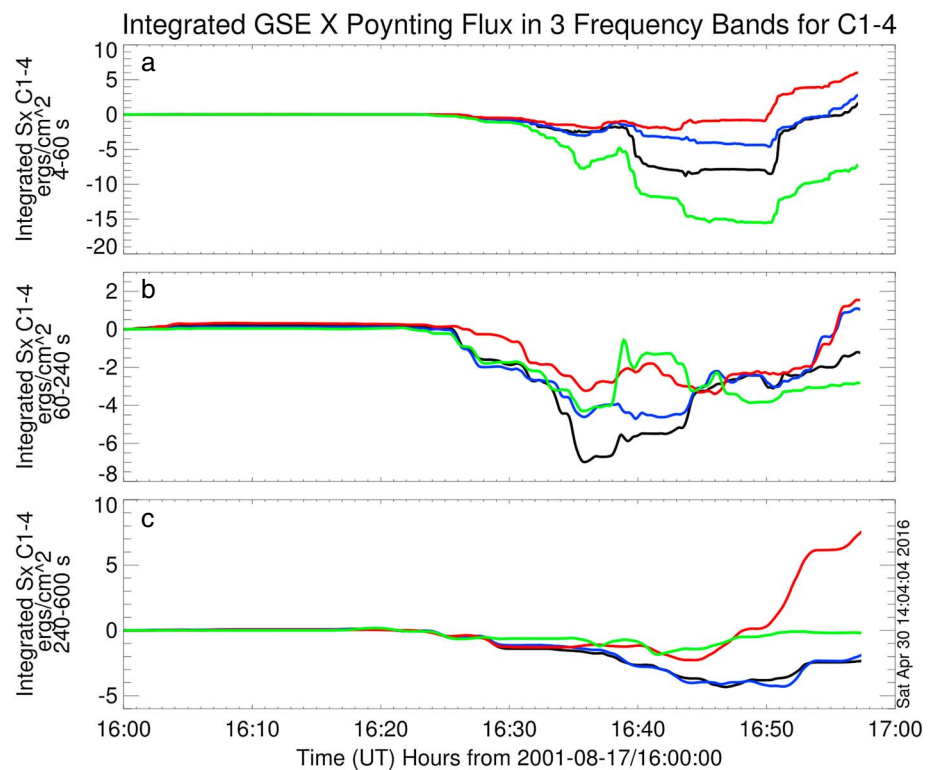


Figure 16. Integrated Poynting flux from 17 August 2001 divided into 4–60 s, 60–240 s, and 240–600 s bands. Spacecraft are distinguished by color (C1 = black, C2 = blue, C3 = red, and C4 = green). Each band on each satellite exhibits significantly different behaviors. The most energy flux is observed in the high-frequency band on average, but the other bands at times dominate on different timescales or on different satellites.

small although the tailward flux seen on C4 is significantly greater than seen on C3. Notably, this is opposite of the behavior of H^+ enthalpy flux, which was seen more strongly on C3 than C4. The spacecraft separation in this case is much less than an O^+ inertial length.

4. Poynting Flux Frequency Bands

We filtered the Poynting flux into different frequency bands in order to isolate the structures and wave types that could be responsible for the energy flux. We look at three frequency bands corresponding to approximate timescales of different phenomena in the tail region. The high-frequency band spans fluctuations from 4 to 60 s of the order of surface waves observed on the current sheet likely driven by Kelvin-Helmholtz instabilities. The midfrequency band spans fluctuations from 60 to 240 s of the order of the flapping timescale of the current sheet. The low-frequency band spans fluctuations from 240 to 600 s, representing large-scale, quasi-static structures in the fields. Figures 14–17 show the integrated Poynting fluxes for each event divided into these three frequency bands. In each figure, panel (a) shows the high-frequency band, panel (b) the mid-frequency band, and panel (c) the low-frequency band, all in the GSE X direction. All four satellites are shown color coded as in Figure 4 in the previous section.

4.1. The 17 August 2003 Event

Filtered integrated Poynting fluxes seen during the 17 August 2003 event are shown in Figure 14. We see that the fluxes observed on all four spacecraft are extremely similar due to the small spacecraft separation. The high-frequency band dominates the total energy flux for all satellites, but the midfrequency flux is comparable in magnitude in both directions. The low-frequency band contributes 2–4 times less to the total energy flux.

Notably there is a significant difference between the tailward-earthward symmetry observed in each of the frequency bands. The high-frequency band shows a slight tailward bias, while the low-frequency band shows a slight earthward bias. On average, the midfrequency band has an equal contribution in each direction. From Figure 4, we saw that the total Poynting flux appeared to be tailward-earthward symmetric. The filtered data

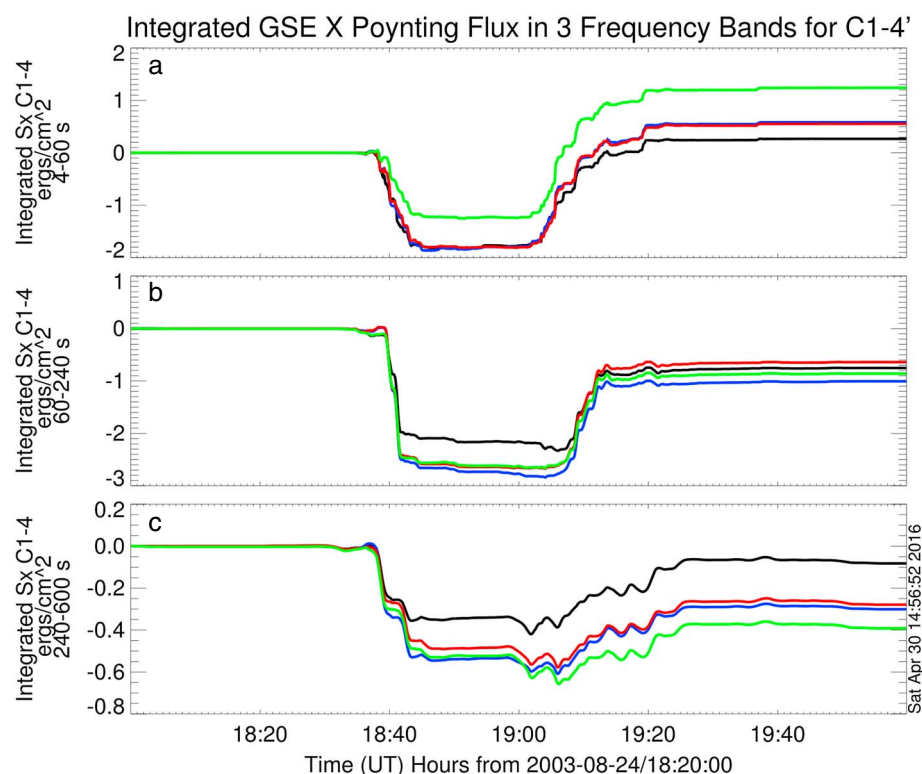


Figure 17. Integrated Poynting flux from 24 August 2003 divided into 4–60 s, 60–240 s, and 240–600 s bands. Spacecraft are distinguished by color (C1 = black, C2 = blue, C3 = red, and C4 = green). Despite the small spacecraft separation, there are differences between the observations on C1 and C4 particularly. Most of the high-frequency flux band is either symmetric or slightly greater earthward, while the other two bands are slightly greater tailward.

show that this does not indicate that the particular waves or structures that are generating Poynting flux are earthward-tailward symmetric.

4.2. 1 October 2001

Filtered integrated Poynting fluxes seen during the 1 October 2001 event are shown in Figure 15. Here we see strikingly different behaviors in the different Poynting flux frequency bands. While the high-frequency energy flux is greater in the earthward direction, the low-frequency component is much stronger in the tailward direction with almost no contribution in the earthward direction on all satellites but C1. The midfrequency band shows a mix of the two behaviors, with C1 demonstrating slightly greater earthward flux and C3 and C4 showing slightly greater tailward flux.

In this event, the satellite separation was large, resulting in significant differences in the fluxes seen on each satellite. Cluster 1 stands out as showing distinct behavior from the other satellites, especially in the middle- and low-frequency bands. From Figure 5, we note that, compared to C4, C1 was further removed from the current sheet and likely was in the lobe region for much of the event. The GSE Z separation between these two satellites was approximately 1000 km. It is also important to note that, during this event, the Cluster fleet observed more current sheet crossings than in any of the other events and *Wygant et al.* [2005] showed that these crossings were due to a flapping motion of the current sheet propagating in the GSE Y direction. Due to this systematic variation of the current sheet normal, our measurements of the Poynting flux will also vary systematically due to the normal electric field shifting in and out of the satellite's plane of measurement.

4.3. The 17 August 2001 Event

Filtered integrated Poynting fluxes seen during the 17 August 2001 event are shown in Figure 16. As in the 1 October 2001 event, we see significant differences between the behavior of the observed energy fluxes in each band. When averaged over all satellites, the high-frequency band dominates the overall flux. However, individual satellites observe very different behaviors. Cluster 4 observes very strong flux in the high-frequency

band and very little flux in the low-frequency band, while the midfrequency band shows a sharp earthward flux structure before the X line crossing that is not observed on any other satellites or frequency bands.

In the low-frequency band, contributions from C1 and C2 are almost exclusively tailward, while contributions from C3 are almost exclusively earthward. In fact, the low-frequency earthward energy flux observed by C3 is stronger than the earthward energy flux of any fluxes seen in the midband and approximately equivalent to the maximum earthward flux seen in the high-frequency band (seen on C1). This is the only event in which the low-frequency band energy fluxes were of the same order as the energy fluxes in the other bands on any satellite.

4.4. The 24 August 2003 Event

Filtered integrated Poynting fluxes seen during the 24 August 2003 event are shown in Figure 17. Again, we see that the tailward-earthward symmetry of the Poynting flux is frequency dependent. The high-frequency Poynting flux band has equal or greater contributions in the earthward direction than the tailward direction on all satellites, but this trend is reversed for the other two frequency bands. The total contributions from the high-frequency and midfrequency Poynting flux bands are very similar, with the midfrequency slightly dominant in the tailward direction and high frequency slightly dominant in the earthward direction. The low-frequency contribution is relatively small in both directions.

Despite the very small spacecraft separation, we observe more variation between spacecraft measurements on 24 August 2003 than in the 17 August 2003 small-separation event. In particular, C1 and C4 tend to observe different fluxes from each other and often the other spacecraft. These two spacecraft are only tens of kilometers apart in GSE X but are separated in GSE Z by approximately 200 km for the duration of the event.

5. Discussion

5.1. Energy Partitioning

The goal of this study was to examine the relative contributions of Poynting flux and species-specific enthalpy and kinetic energy fluxes to the total energy leaving the reconnection region. *Eastwood et al.* [2013] concluded that ion enthalpy flux was dominant, followed by electron enthalpy, with Poynting flux being significant in some cases. Computer simulations by *Birn and Hesse* [2010] indicate that, in the presence of a guide field, redirected Poynting flux is likely to be significant and that otherwise the majority of energy released is converted into ion enthalpy flux. However, these studies were unable to include electron energy fluxes. *Yamada et al.* [2015] indicates that Poynting flux accounts for the majority of energy outflow, followed by the ion enthalpy flux and electron enthalpy flux, using both PIC simulations and lab plasma experiments. However, they note that these results are not in agreement with observations in the space environment. None of the above studies examined ion species, integrated fluxes, or distinguished the different structures which might be sources of Poynting flux.

Studying each event individually reveals a large variability in the energy partitioning, both spatially, temporally, and between events. Figure 18 summarizes the integrated Poynting flux, electron enthalpy flux, O⁺ enthalpy flux, H⁺ enthalpy flux, and H⁺ kinetic energy flux for each event, tailward and earthward. The electron and O⁺ kinetic energy fluxes were not included due to being negligible in all events. The tailward flux on each satellite was determined by measuring the maximum integrated energy flux in the tailward direction seen prior to the approximated crossing of the X line. Similarly, the earthward flux was determined by measuring the maximum integrated energy flux in the earthward direction seen after the crossing of the X line.

Figure 18a displays the integrated energy fluxes for the event on 17 August 2003, Figure 18b on 1 October 2001, Figure 18c on 17 August 2001, and Figure 18d 24 August 2003. The tailward flows are plotted as negative, and the earthward flows are plotted as positive. For energy fluxes measured on more than one satellite, the length of the bar indicates the range of values from the satellite observing the least integrated energy flux to the satellite that observes the greatest. Measurements marked with a star were observed by one satellite only.

In all cases, the average H⁺ flux in the tailward direction was larger than any other energy flux in that direction. However, other contributions to the tailward flux were not negligible. The electron enthalpy flux in the tailward direction was often comparable to the minimum observed tailward H⁺ enthalpy flux. In the 1 October 2001 event in particular, the tailward electron enthalpy flux was nearly identical to the tailward H⁺ enthalpy flux. The electron enthalpy flux was characterized by short timescale, strong bursts of flux reaching several times the typical peak values of the H⁺ enthalpy flux. In contrast, the H⁺ enthalpy flux was characterized by

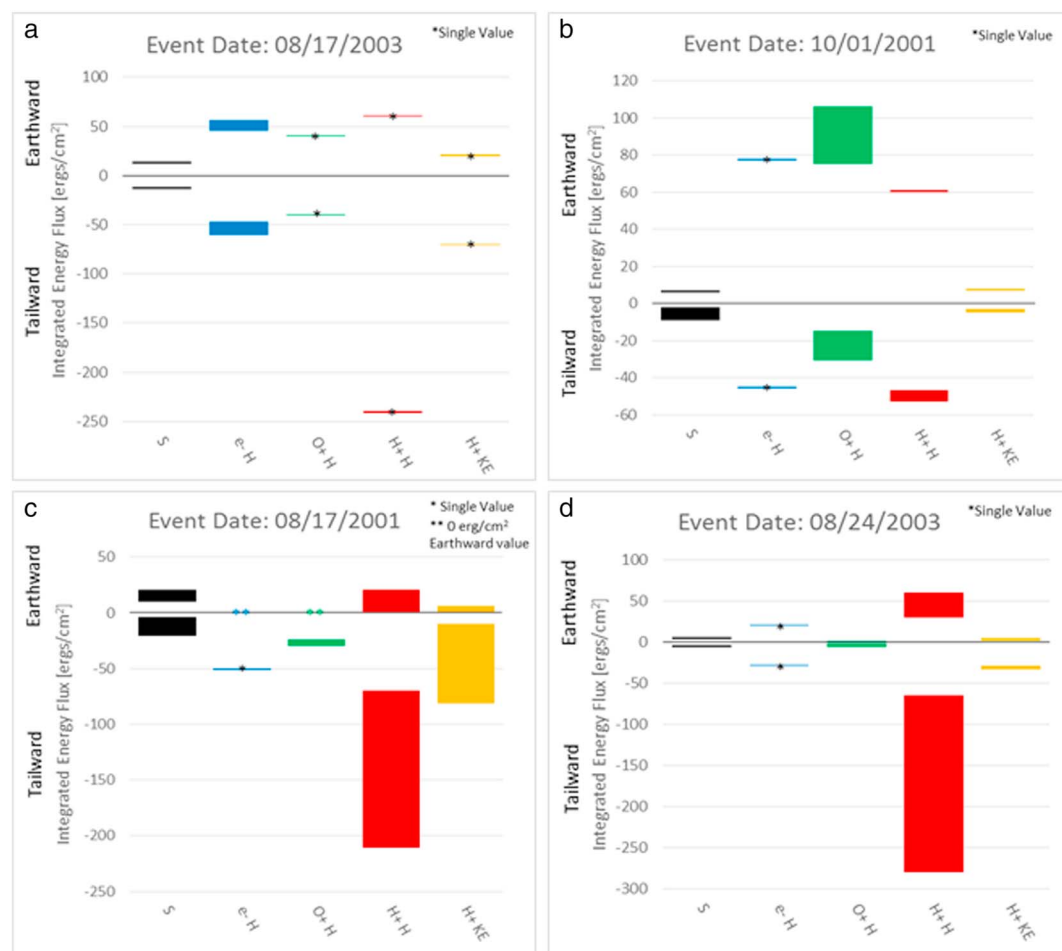


Figure 18. Above is a visualization of the magnitude and range of integrated energy fluxes in the earthward and tailward direction during the four events. The results for (a) the event on 17 August 2003, (b) the event on 1 October 2001, (c) the event on 17 August 2001, and (d) the event on 24 August 2003. From left to right, the color bars represent integrated Poynting flux, electron enthalpy flux, O⁺ enthalpy flux, H⁺ enthalpy flux, and H⁺ kinetic energy flux. Negative values indicate the tailward direction, and positive values indicate the earthward direction. Many values are represented by a bar which spans the minimum value obtained by any one satellite during that event to the maximum value obtained by any one satellite during that event. Values marked with stars were only observed on a single satellite.

more sustained energy fluxes with lower peak values. The Poynting flux in the tailward direction was always relatively small, often more than an order of magnitude smaller than the maximum tailward H⁺ enthalpy flux. The tailward H⁺ kinetic energy flux varied significantly between events, ranging from approximately 3 times smaller than the H⁺ enthalpy flux on 17 August 2003 and 17 August 2001 to more than an order of magnitude smaller on 1 October 2001. Satellites that measured strong H⁺ enthalpy flux tended to measure strong H⁺ kinetic energy flux as well.

The partitioning of the energy flux in the earthward direction, however, looked quite different than the partitioning in the tailward direction. The H⁺ enthalpy flux was no longer the dominant contributor to the overall energy budget in all cases. During the 1 October 2001 event, both the O⁺ enthalpy flux and the e⁻ enthalpy flux exceeded the earthward H⁺ enthalpy flux. On 17 August 2003 the e⁻ enthalpy was approximately equivalent to the H⁺ enthalpy flux. And on 17 August 2001 the Poynting flux was approximately equivalent to the H⁺ enthalpy flux. This difference between the tailward and earthward dominance of the H⁺ enthalpy flux is indicative of an asymmetry between the amount of tailward and earthward energization of the H⁺ ions. This asymmetry was seen also in the H⁺ kinetic energy flux and, in general, is not seen in the Poynting flux, electron enthalpy flux, or oxygen enthalpy flux.

The X line during magnetotail reconnection retreats tailward from where reconnection was initiated. We recognized that this tailward motion could contribute to the asymmetry observed in H⁺ energy fluxes due to measurements being taken in the satellite frame rather than the moving frame of the X line. However, the speed of the X line estimated in a study of the 1 October 2001 event [Imada *et al.*, 2007] and in an MHD simulation [Kuznetsova *et al.*, 2007] is approximately 100 km/s, which is much less than the ion speeds observed (up to 1300 km/s). Furthermore, if the asymmetry were primarily caused by the motion of the X line, we would expect to see a much stronger asymmetry in the H⁺ kinetic energy flux than the H⁺ enthalpy flux, but this is not what we observe. We conclude that the tailward retreat of the X line is a negligible contribution to the observed asymmetry. The common explanation for the tailward-earthward asymmetry is the nonsymmetric boundary conditions on the earthward and tailward side of the reconnection region due to higher densities and closed field lines near the Earth [Cattell *et al.*, 1992; Shiokawa *et al.*, 1997]. The resistive MHD study from Birn and Hesse [2005] showed both a proton braking effect and a reduction of H⁺ enthalpy flux earthward of the X line due to field dipolarization which might account for our observations. However, the enthalpy flux reduction occurred roughly 10 R_E earthward from the reconnection region in the simulations, which is not consistent with our observations close to the X line.

Part of the inherent value of using the Cluster spacecraft for this analysis is the ability to observe the same event simultaneously on different spacecraft over a range of spacecraft separations. We observed highly disparate behavior in the tailward H⁺ enthalpy flux between satellites in two of the three events in which we had more than one satellite measurement. During these events, we observed approximately 3–4 times as much integrated energy flux on one satellite as the other. Surprisingly, this disparity was observed both during a large spacecraft separation event (17 August 2001) and small separation event (24 August 2003). Also notable is that the H⁺ kinetic energy flux on 24 August 2003 did not show the same disparity as the H⁺ enthalpy flux. The variability that we see on such small spatial scales indicates that the heating of H⁺ ions is significantly impacted by microphysical processes, resulting in highly localized energy flows. In contrast, the Poynting flux measurements are relatively similar between satellites. The electron enthalpy, unfortunately, is observed on only one satellite in all but the 17 August 2003 event, making it impossible to draw general conclusions about the spatial scales of electron energization. During this one event, however, the variations between satellites were only on the order of 20–30% of the average flux value.

Because previous energy partitioning studies have not separated ion species, the oxygen behavior was of particular interest. The O⁺ ion enthalpy does not show the systematic asymmetry of the H⁺ enthalpy. In fact, the O⁺ enthalpy flux differs significantly in behavior from the H⁺ enthalpy flux in all four events, either in the dominant direction of the energy flow or in discrepancies observed between satellites. This indicates that the energization mechanisms and spatial extent of the energization of O⁺ ions are entirely different from H⁺ ions, due to differences in gyroradii. As discussed in Markidis *et al.* [2011], this also causes a spatial species separation which may account for some of the differences in the H⁺ and O⁺ fluxes seen on different spacecraft. The discrepancy between H⁺ and O⁺ enthalpy observations on C3 and C4 on 24 August 2003 indicates that these differences can be observed even over very small scales, less than an O⁺ inertial length.

During the 1 October 2001 event, the earthward O⁺ enthalpy flux is the dominant energy flux, exceeding both the e⁻ and H⁺ enthalpy. Wygant *et al.* [2005] examined the O⁺ distribution functions during this event around 9:47 UT and noted strong, counter-streaming jets accelerated by the large potential drop across the current sheet. Because their gyroradii are larger than the current sheet structure, O⁺ ions undergo electrostatic acceleration, while H⁺ ions, with gyroradii smaller than the current sheet structure, will $E \times B$ drift toward the center of the structure. This mechanism is further supported by PIC simulations of oxygen energization performed by Liang *et al.* [2016] which demonstrate large oxygen enthalpy fluxes in the downstream region not associated with large H⁺ enthalpy flux. The 1 October 2001 event occurred during a prolonged period of negative *Dst* and high *AE* which is generally associated with higher O⁺ densities in the magnetosphere and thus may contribute to the strong O⁺ enthalpy flux seen in this event. The 24 August 2003 event also occurred after prolonged negative *Dst*, but the *AE* index observed in the hours immediately before this event were lower than the values seen on 1 October 2001. This may contribute to the fact that the resultant O⁺ energy fluxes did not contribute any significant portion of the overall energy.

In two of the events, ion enthalpy and kinetic energy flux bursts, were seen earlier than the majority of the Poynting flux and electron activity. These bursts were associated with field-aligned ion flows and contributed significantly to the total ion enthalpy and kinetic energy fluxes. The fact that these flows were not seen in all

events may be a result of whether the spacecraft fleet was positioned near the plasma sheet boundary where such flows would be observed.

5.2. Poynting Flux Frequency Bands

The Poynting flux was filtered into different frequency bands in an attempt to isolate the structures and wave types that could be responsible for the energy flux. Figure 19 summarizes the Poynting flux in each of the three frequency bands observed in the tailward and earthward directions. The method of quantifying the fluxes and presenting the value ranges is analogous to Figure 18. We find that the high-frequency and midfrequency bands tend to have comparable flux values in both directions, while the low-frequency band is generally a few times smaller in value. We conclude that quasi-static, large-scale structures generally contribute less to the overall energy than smaller timescale fluctuations. The exception was seen on 17 August 2001, when C3 observed an earthward flux in the low-frequency band that was comparable to the maximum flux seen in the high-frequency band and twice that of the maximum flux seen in the midfrequency band.

In Wygant *et al.* [2005], the crossing of a bifurcated current sheet was studied during the 1 October 2001 event. This crossing was observed via strong bipolar signatures of a Hall electric field crossing around 9:47 UT. The timescale of this crossing varied depending on the satellites' proximity to the X line, from 6 s (observed on Cluster 4) to 25 s (observed on Cluster 3). Of interest in this study was whether these Hall signatures contributed significantly to the Poynting flux. We compared the time of the current sheet crossing in Wygant *et al.* to the high-frequency filtered Poynting flux. Only Cluster 3 showed a significant integrated flux increase (~ 1.2 ergs/cm²) which might be associated with this crossing. However, because of the short timescales involved in this current sheet crossing, it is likely that our high-frequency band still has too low of a sampling rate to accurately represent the Poynting flux contribution from this feature on the other satellites. Alternatively, the short duration of the other satellite crossings may have caused the time-integrated contribution of the event to be negligible in the frame of the spacecraft.

Dai *et al.* [2011] presents an analysis of Kelvin-Helmholtz-driven surface waves confined to the current sheet during the 17 August 2003 event. These surface waves ranged in frequency between 0.03 Hz and 1 Hz, corresponding to the 4–60 s band in this paper. Dai's analysis of the power spectrum of these waves yielded Poynting flux values of ≈ 0.1 ergs/cm²/s which is comparable within a factor of 2 with peak values in the high-frequency band observed in each of the events in this paper. However, plasma-sheet-confined waves would be expected to diminish significantly in amplitude when the spacecraft enters the lobe region. Because of the small spacecraft separation during this event, it is not possible to obtain simultaneous measurements of the Poynting flux close to the current sheet and in the lobe. This distinction is easier to make during the 17 August 2001 event with a large spacecraft separation. Here we have indications from B_x measurements and tailward H⁺ velocities that C4 is frequently close to the current sheet on the tailward side of the X line and C1 is more often in the lobe region (see Figure 8). C4 subsequently shows a larger tailward flux and a comparable earthward flux to C1 in the high-frequency band. This behavior is not seen in the other two frequency bands, indicating that surface waves similar to those seen by Dai *et al.* may be present and strongly contributing to the Poynting flux on 17 August 2001 as well.

Current sheet "flapping" describes the persistent wave-like motion seen in the plasma sheet enhanced during storm conditions. These motions tend to have periods of the order of minutes [Sergeev *et al.*, 2003; Runov *et al.*, 2005]. Wygant *et al.* [2005] also performed timing analysis on the current sheet crossings observed during the 1 October 2001 event and determined that the satellite fleet was observing a flapping of the current sheet propagating in the GSE Y direction with a period on the order of a minute. These waves primarily fall within the midfrequency band, which contributes significantly to the total Poynting flux in all events. Thus, we conclude that waves associated with current sheet flapping may be a significant source of Poynting flux. Notably, in the 17 August 2001 event, C4 (which is closer to the current sheet than C1) sees a sudden earthward flux in this frequency band that is not seen on any of the other satellites or in any of the other frequency bands. The origin of this feature is unknown.

The largest timescale that was analyzed was the 240–600 s band, which primarily corresponds to large-scale and quasi-static structures. This band was consistently shown to contribute less Poynting flux than the other two bands, with only the exception of observations on C3 during the 17 August 2001 event. Unfortunately, due to a lack of ion data and reliable density data from spacecraft potential on C3, it is difficult to ascertain what region this satellite was in and why it might be observing a different structure than the other spacecraft. In all

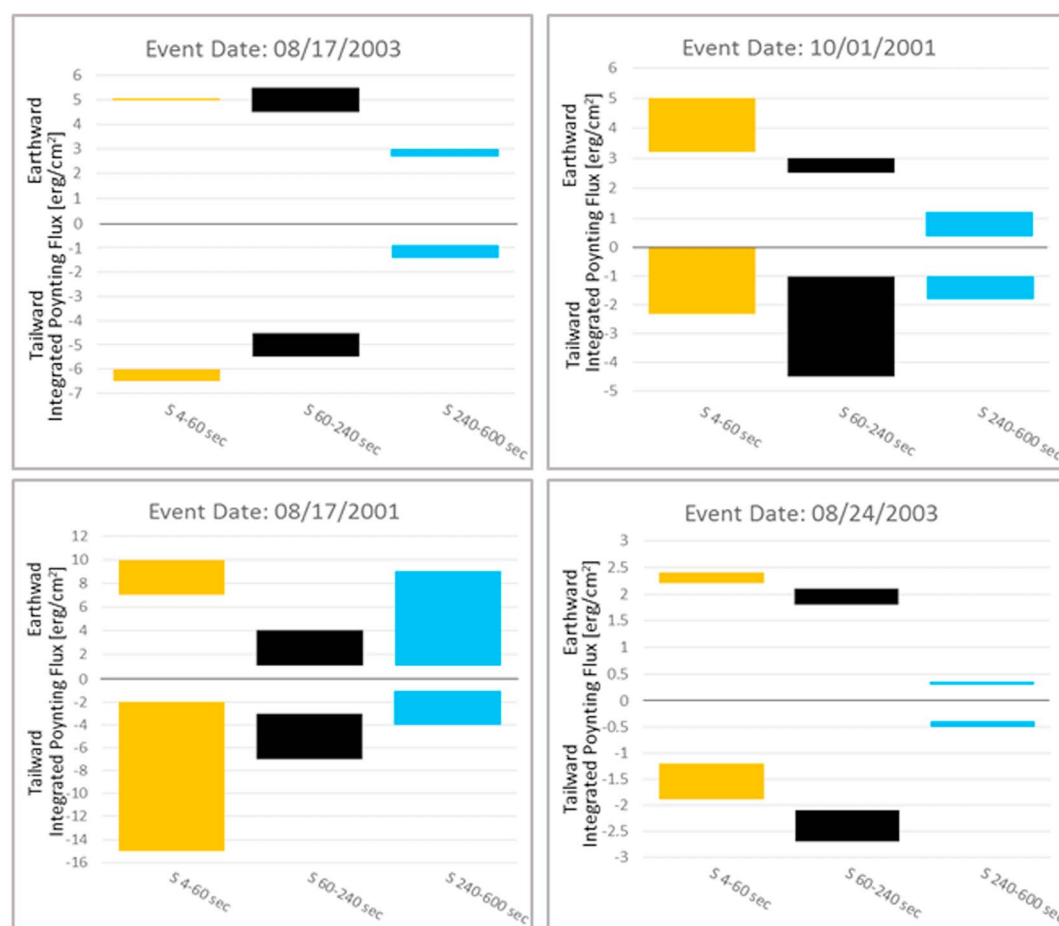


Figure 19. Above is a visualization of the magnitude and range of frequency-filtered integrated Poynting fluxes in the earthward and tailward direction during the four events. From left to right, the color bars represent the 4–60 s band, the 60–240 s band, and the 240–600 s band. Negative values indicate the tailward direction and positive values indicate the earthward direction. The values are represented by a bar which spans the minimum value obtained by any one satellite during that event to the maximum value obtained by any one satellite during that event.

other cases, however, we conclude that large-scale and quasi-static structures are generally not a significant generator of Poynting flux.

6. Summary and Conclusions

We have presented the results of our study of integrated energy outflow during four magnetotail reconnection events observed by the Cluster spacecraft in 2001 and 2003. Our primary focus was twofold: to perform a detailed comparison of the contribution of energy fluxes tailward and earthward from the X line and to examine the Poynting flux in different frequency bands to attempt to isolate possible underlying mechanisms. A summary of our observations is listed below.

1. We confirmed previous results that H⁺ enthalpy flux is often the dominant energy flux [Aunai *et al.*, 2011; Birn and Hesse, 2005; Eastwood *et al.*, 2013]. However, we found that electron enthalpy flux, Poynting flux, H⁺ kinetic energy flux, and O⁺ enthalpy flux can contribute significantly and, in some cases, more than the H⁺ enthalpy flux depending on the relative position of the spacecraft in relation to the plasma sheet boundary, the flow direction, and the event being studied.
2. Large differences were seen between H⁺ enthalpy fluxes measured on different satellites in two of the three events in which we had measurements from more than one satellite. In the 17 August 2001 event, the difference could be attributed to C4 being positioned closer to the plasma sheet than C1. However, during the 24 August 2003 event, no significant difference in the plasma conditions between C3 (observing large H⁺ enthalpy flux) and C4 (observing small H⁺ enthalpy flux) were observed and the satellite separation

was only one the order of a proton inertial length. This result implies that microphysical processes that may energize protons in these regions are extremely localized.

3. We observed a earthward-tailward asymmetry in the proton-associated fluxes in three of the four events with greater flux seen in the tailward direction. This difference was observed to be up to approximately 6 times greater integrated flux tailward than earthward on 17 August 2003. A similar statistical tailward-earthward asymmetry was noted in *Eastwood et al.* [2013]. This bias may be related to the different boundary conditions between the open tail side and the closed Earth side of the system, but this is difficult to study in simulations. *Birn and Hesse* [2005] demonstrated a deenergizing effect on the earthward side of the reconnection line with resistive MHD simulations caused by dipolarization, but this occurred further earthward than our observations.
4. We observed significant differences in behavior between the O⁺ enthalpy flux and the H⁺ enthalpy flux in all four of the studied events. In the 17 August 2001 and 24 August 2003 events, we observed spatial structures in the H⁺ flux that differed from those seen in the O⁺ flux by comparison of multiple satellite measurements. During the 17 August 2003 event, the tailward-earthward asymmetry in the H⁺ enthalpy flux was not observed in the O⁺ enthalpy flux. Finally, in the 1 October 2001 event, the O⁺ enthalpy flux demonstrates a strong earthward flux not seen in the H⁺ enthalpy flux. We conclude that the O⁺ ion behavior is significantly different from proton behavior due to differences between their gyroradii and inertial lengths. This results in the two ions being accelerated over different scales and by different structures.
5. We observed O⁺ enthalpy flux to be greater than all other fluxes in the earthward direction during the 1 October 2001 event. This indicates that energy contributions due to oxygen ions cannot be ignored in analysis of the energy outflows from tail reconnection and that their energization mechanisms are distinct from H⁺ ions.
6. We found that Poynting flux frequency bands associated with plasma sheet surface waves and the drivers of plasma sheet flapping contribute most significantly to the overall earthward and tailward Poynting flux. Large-scale structures contribute relatively little to the overall Poynting flux in almost all cases.
7. We observed significant differences between the behavior of the Poynting flux in each of the three studied frequency bands, implying that the overall observed Poynting flux is a complex superposition of different structures and waves which vary spatially and temporally with respect to each other and may at times generate Poynting flux in opposite directions.
8. We found that the Poynting flux is often very symmetric in the tailward-earthward direction, but that individual frequency bands frequently show directional asymmetries. The directional asymmetries of each band are often opposed to each other, resulting in symmetric total Poynting flux.

From this analysis, we conclude that the behaviors observed imply complex energization mechanisms which are at present poorly understood. The spatial variation of the energization of particles in these events implies that energization can occur on very small scales, within a single ion inertial length. We also find a tailward-earthward asymmetry in the H⁺ ion flows which we attribute to the different boundary conditions in the downstream regions. This asymmetry has been noted previously but is, as yet, poorly understood, and large-scale simulations are able to obtain these results only on much further from the X line than we observe.

We find that electron enthalpy is a significant contribution to the overall energy flux, especially over short temporal or spatial scales and in the tailward direction. Since many simulations are unable to simulate electron contributions due to computational limitations, it should be recognized that significant energy contributions will be unaccounted for. We also see a strong case for further study of the behavior and influence of O⁺ ions in the reconnection region of the magnetotail and their contributions to the energy outflow in these regions. We find that in some situations the energy contribution from O⁺ enthalpy is not negligible.

Finally, the varied behavior observed in the frequency-filtered Poynting flux indicates multiple of sources of Poynting flux from reconnection regions. Our analysis concluded that large-scale structures are relatively insignificant sources of Poynting flux, while surface waves and sources of current sheet flapping are significant. However, due to limitations in our measurements of the electric field our results are incomplete, especially in cases where the current sheet topology is known to be changing. Simulations of Poynting flux from reconnection may be able to further detangle the superposition of waves and structures we observe without these measurement limitations.

Acknowledgments

We would like to thank the Cluster spacecraft software and engineering teams for making these data available. We gratefully acknowledge Alexander Igl for his assistance with some graphics. This work was supported by NASA grant NNX13AE16G at the University of Minnesota, Twin Cities. Cluster data can be accessed from the ESA Cluster Science Archive (<http://www.cosmos.esa.int/web/csa>).

References

- Asano, Y., et al. (2008), Electron flat-top distributions around the magnetic reconnection region, *J. Geophys. Res.*, **113**, A01207, doi:10.1029/2007JA012461.
- Aunai, N., G. Belmont, and R. Smets (2011), Energy budgets in collisionless magnetic reconnection: Ion heating and bulk acceleration, *Phys. Plasmas*, **18**, 122901, doi:10.1063/1.3664320.
- Balogh, A., et al. (2001), The cluster magnetic field investigation: Overview of in-flight performance and initial results, *Ann. Geophys.*, **19**, 1207–1217, doi:10.5194/angeo-19-1207-2001.
- Birn, J., and M. Hesse (2005), Energy release and conversion by reconnection in the magnetotail, *Ann. Geophys.*, **23**, 3365–3373, doi:10.5194/angeo-23-3365-2005.
- Birn, J., and M. Hesse (2010), Energy release and transfer in guide field reconnection, *Phys. Plasmas*, **17**, 012109, doi:10.1063/1.3299388.
- Cattell, C., C. Carlson, W. Baumjohann, and H. Lühr (1992), The MHD structure of the plasmasheet boundary: (1) Tangential momentum balance and consistency with slow mode shocks, *Geophys. Res. Lett.*, **19**, 2083–2086, doi:10.1029/92GL02181.
- Cattell, C., et al. (2005), Cluster observations of electron holes in association with magnetotail reconnection and comparison to simulations, *J. Geophys. Res.*, **110**, A01211, doi:10.1029/2004JA010519.
- Cattell, C., et al. (2011), Observations of a high-latitude stable electron auroral emission at ~16 MLT during a large substorm, *J. Geophys. Res.*, **116**, A07215, doi:10.1029/2010JA016132.
- Dai, L., J. R. Wygant, C. Cattell, J. Dombeck, S. Thaller, C. Moukikis, A. Balogh, and H. Rème (2011), Cluster observations of surface waves in the ion jets from magnetotail reconnection, *J. Geophys. Res.*, **116**, A12227, doi:10.1029/2011JA017004.
- Eastwood, J. P., T. D. Phan, M. Øieroset, and M. A. Shay (2010), Average properties of the magnetic reconnection ion diffusion region in the Earth's magnetotail: The 2001–2005 Cluster observations and comparison with simulations, *J. Geophys. Res.*, **115**, A08215, doi:10.1029/2009JA014962.
- Eastwood, J. P., T. D. Phan, J. F. Drake, M. A. Shay, A. L. Borg, B. Lavraud, and M. G. T. Taylor (2013), Energy partition in magnetic reconnection in Earth's magnetotail, *Phys. Rev. Lett.*, **110**, 225001, doi:10.1103/PhysRevLett.110.225001.
- Goldman, M. V., D. L. Newman, and G. Lapenta (2016), What can we learn about magnetotail reconnection from 2D PIC harris-sheet simulations?, *Space Sci. Rev.*, **199**, 651–688, doi:10.1007/s11214-015-0154-y.
- Gustafsson, G., et al. (1997), The electric field and wave experiment for the cluster mission, in *The Cluster and Phoenix Missions*, edited by C. P. Escoubet, C. T. Russell, and R. Schmidt, pp. 137–156, Springer, Netherlands, doi:10.1007/978-94-011-5666-0.
- Henderson, P. D., C. J. Owen, A. D. Lahiff, I. V. Alexeev, A. N. Fazakerley, E. Lucek, and H. Rème (2006), Cluster PEACE observations of electron pressure tensor divergence in the magnetotail, *Geophys. Res. Lett.*, **33**, L22106, doi:10.1029/2006GL027868.
- Hones, E. W. (1976), Observations in the Earth's magnetotail relating to magnetic merging, *Sol. Phys.*, **47**, 101–113, doi:10.1007/BF00152248.
- Imada, S., R. Nakamura, P. W. Daly, M. Hoshino, W. Baumjohann, S. Mühlbachler, A. Balogh, and H. Rème (2007), Energetic electron acceleration in the downstream reconnection outflow region, *J. Geophys. Res.*, **112**, A03202, doi:10.1029/2006JA011847.
- Johnstone, A. D., et al. (1997), PEACE: A plasma electron and current experiment, *Space Sci. Rev.*, **79**, 351–398, doi:10.1023/A:1004938001388.
- Kistler, L. M., et al. (2005), Contribution of nonadiabatic ions to the cross-tail current in an O⁺ dominated thin current sheet, *J. Geophys. Res.*, **110**, A06213, doi:10.1029/2004JA010653.
- Kuznetsova, M. M., M. Hesse, L. Rastätter, A. Taktakishvili, G. Toth, D. L. De Zeeuw, A. Ridley, and T. I. Gombosi (2007), Multiscale modeling of magnetospheric reconnection, *J. Geophys. Res.*, **112**, A10210, doi:10.1029/2007JA012316.
- Liang, H., G. Lapenta, R. Walker, M. El-Alaoui, and J. Berchem (2016), Acceleration of oxygen ions in the magnetotail near and far away from the reconnection region, Poster session presented at Geospace Environment Modeling, Santa Fe, N. M.
- Markidis, S., G. Lapenta, L. Bettarini, M. Goldman, D. Newman, and L. Andersson (2011), Kinetic simulations of magnetic reconnection in presence of a background O⁺ population, *J. Geophys. Res.*, **116**, A00K16, doi:10.1029/2011JA016429.
- Mozar, F. S., S. D. Bale, and T. D. Phan (2002), Evidence of diffusion regions at a subsolar magnetopause crossing, *Phys. Rev. Lett.*, **89**, 015002, doi:10.1103/PhysRevLett.89.015002.
- Nakamura, R., W. Baumjohann, Y. Asano, A. Runov, A. Balogh, C. J. Owen, A. N. Fazakerley, M. Fujimoto, B. Klecker, and H. Rème (2006), Dynamics of thin current sheets associated with magnetotail reconnection, *J. Geophys. Res.*, **111**, A11206, doi:10.1029/2006JA011706.
- Øieroset, M., T. D. Phan, M. Fujimoto, R. P. Lin, and R. P. Lepping (2001), In situ detection of collisionless reconnection in the Earth's magnetotail, *Nature*, **412**, 414–417, doi:10.1038/35086520.
- Rème, H., et al. (1997), The Cluster Ion Spectrometry (CIS) experiment, in *The Cluster and Phoenix Missions*, edited by C. P. Escoubet, C. T. Russell, and R. Schmidt, pp. 303–350, Springer, Netherlands, doi:10.1007/978-94-011-5666-0.
- Runov, A., et al. (2003), Current sheet structure near magnetic X-line observed by Cluster, *Geophys. Res. Lett.*, **30**(11), 1579, doi:10.1029/2002GL016730.
- Runov, A., et al. (2005), Electric current and magnetic field geometry in flapping magnetotail current sheets, *Ann. Geophys.*, **23**, 1391–1403, doi:10.5194/angeo-23-1391-2005.
- Sergeev, V., et al. (2003), Current sheet flapping motion and structure observed by Cluster, *Geophys. Res. Lett.*, **30**(6), 1327, doi:10.1029/2002GL016500.
- Shiokawa, K., W. Baumjohann, and G. Haerendel (1997), Braking of high-speed flows in the near-Earth tail, *Geophys. Res. Lett.*, **24**, 1179–1182, doi:10.1029/97GL01062.
- Sonnerup, B. U., G. Paschmann, I. Papamastorakis, N. Sckopke, G. Haerendel, S. J. Bame, J. R. Asbridge, J. T. Gosling, and C. T. Russell (1981), Evidence for magnetic field reconnection at the Earth's magnetopause, *J. Geophys. Res.*, **86**(A12), 10,049–10,067, doi:10.1029/JA086iA12p10049.
- Wygant, J. R., et al. (2005), Cluster observations of an intense normal component of the electric field at a thin reconnecting current sheet in the tail and its role in the shock-like acceleration of the ion fluid into the separatrix region, *J. Geophys. Res.*, **110**, A09206, doi:10.1029/2004JA010708.
- Yamada, M., J. Yoo, J. Jara-Almonte, W. Daughton, H. Ji, R. Kulsrud, and C. Myers (2015), Study of energy conversion and partitioning in the magnetic reconnection layer of a laboratory plasma, *Phys. Plasmas*, **22**, 056501, doi:10.1063/1.4920960.